Increased Transnational Sea Ice Transport Between Neighboring Arctic States in the 21st Century

Patricia DeRepentigny[1,2], Alexandra Jahn[1], L. Bruno Tremblay[2,3], Robert Newton[3], and Stephanie Pfirman[4]

[1]Department of Atmospheric and Oceanic Sciences and Institute of Arctic and Alpine Research, University of Colorado Boulder, Boulder, Colorado, USA.
[2]Department of Atmospheric and Oceanic Sciences, McGill University, Montreal, Quebec, Canada.
[3]Lamont-Doherty Earth Observatory, Columbia University, Palisades, New York, USA.
[4]School of Sustainability, Arizona State University, Tempe, Arizona, USA.

Key Points:

- The CESM projects a large increase in transnational ice exchanged in the Arctic by mid-century with transit times reduced to under two years
- By mid-century the amount of transnational ice originating from Russia doubles and the Central Arctic emerges as the second dominant source
- Long-distance ice transport pathways disappear by 2100 in favor of regions directly downstream, especially under the high emissions scenario

An edited version of this paper was published by AGU. Copyright (2020) American Geophysical Union. Citation: DeRepentigny, P., Jahn, A., Tremblay, L. B., Newton, R., and Pfirman, S. (2020). Increased Transnational Sea Ice Transport Between Neighboring Arctic States in the 21st Century. *Earth's Future*, 8, e2019EF001284. https://doi.org/10.1029/2019EF001284

Corresponding author: Patricia DeRepentigny, `patricia.derepentigny@colorado.edu`

Abstract

The Arctic is undergoing a rapid transition toward a seasonal ice regime, with widespread implications for the polar ecosystem, human activities, as well as the global climate. Here we focus on how the changing ice cover impacts trans-border exchange of sea ice between the exclusive economic zones of the Arctic states. We use the Sea Ice Tracking Utility (SITU), which follows ice floes from formation to melt, in conjunction with output diagnostics from two ensembles of the Community Earth System Model (CESM) that follow different future emissions scenarios. The CESM projects that by mid-century, transnational ice exchange will more than triple, with the largest increase in the amount of transnational ice originating from Russia and the Central Arctic. However, long-distance ice transport pathways are predicted to diminish in favor of ice exchanged between neighboring countries. By the end of the 21^{st} century, we see a large difference between the two future emissions scenarios considered: consistent nearly ice-free summers under the high emissions scenario act to reduce the total fraction of transnational ice exchange compared to mid-century, whereas the low emissions scenario continues to see an increase in the proportion of transnational ice. Under both scenarios, transit times are predicted to decrease to less than two years by 2100, compared to a maximum of six years under present-day conditions and two and a half years by mid-century. These significant changes in ice exchange and transit time raise important concerns regarding risks associated with ice-rafted contaminants.

Plain Language Summary

The Arctic is undergoing a rapid transition toward a thinner, less extensive, more mobile sea ice cover. This affects the amount of sea ice exchanged between the exclusive economic zones of Arctic states. Here we use an Earth System Model, the Community Earth System Model (CESM), to track sea ice from where it forms to where it ultimately melts. By mid-century, the area of sea ice exchanged between the different regions of the Arctic is predicted to more than triple compared to the end of the 20^{th} century, with the Central Arctic joining Russia as a major ice "exporter". At the same time, the exchange of sea ice over long distances is predicted to diminish in favor of ice exchanged between neighboring Arctic states. By mid-century, the average time required for ice to travel from one region to another is more than halved; by 2100, nearly all transports take less than a year, with little multi-year ice left in the Arctic. Sea ice provides a transport mechanism for a variety of material, including algae, dust and a range of pollutants. The acceleration, and then disappearance, of sea ice has important implications for managing contamination in Arctic waters.

1 Introduction

The Arctic sea ice cover has been retreating over the past four decades and is predicted to continue to decline throughout the 21st century (e.g., SIMIP Community, 2020; Stroeve, Kattsov, et al., 2012; Stroeve & Notz, 2018). Sea ice loss provides easier marine access to the Arctic and great opportunities for economic activities (Aksenov et al., 2017; Ng et al., 2018; Schøyen & Bråthen, 2011; Stephenson et al., 2013), but is also associated with growing risks and emerging political tensions (Arctic Council, 2009; Emmerson & Lahn, 2012; Newton et al., 2016). When ice concentrations are high, sea ice can raft various materials, including pollutants, and transport them much farther than ocean currents across the Arctic basin (Blanken et al., 2017). Newton et al. (2017) have shown that the total area of sea ice exchanged across the Arctic Ocean has been increasing over the historical period as a result of sea ice retreat and thinning, with higher ice drift speeds and associated shorter transit times between different regions. However, long-range transport of sea ice and ice-rafted material has started to decrease in recent years due to intensified melt in the marginal ice zones of the Arctic Ocean (Krumpen et al., 2019; Newton et al., 2017). It is currently unclear how transnational ice exchange will evolve in the future as the Arctic continues to transition toward a seasonally ice-free state, in particular when considering the competing effects of increased drift speeds versus shorter periods for sea ice to transit the Arctic as the melt season lengthens. In this study, we investigate how transnational sea ice exchange between the different Arctic states is predicted to change during the 21st century using the Community Earth System Model (CESM1; Hurrell et al., 2013).

September sea ice extent has been declining at a rate of roughly 11% per decade since the start of the satellite era in 1979 (Comiso et al., 2017; Stroeve & Notz, 2018) and there is evidence that the rate of decline has accelerated since the beginning of the 21st century (Comiso et al., 2008; Ogi & Rigor, 2013; Stroeve, Serreze, et al., 2012). In addition, there has been an increase in the length of the open-water season in the Arctic over recent decades (Barnhart et al., 2016; Smith & Jahn, 2019; Stroeve, Markus, et al., 2014) and the sea ice cover has undergone substantial thinning with a considerable decline in the amount of multi-year ice (Comiso, 2012; Kwok, 2018; Stroeve, Barrett, et al., 2014; Stroeve & Notz, 2018). The retreat of Arctic sea ice combined with more extensive open-water periods have modified interactions between the different stakeholders of the High North, raising new political issues and heightening potential conflicts among Arctic states (Emmerson & Lahn, 2012; Newton et al., 2016; Wilhelmsen & Gjerde, 2018). Current model projections suggest that nearly ice-free summers, defined as ice extent that falls below one million km^2, are very likely unless warming is limited to 1.5°C (Jahn, 2018; Niederdrenk & Notz, 2018; Screen & Williamson, 2017; Sigmond et al., 2018). It has been shown that if emissions of anthropogenic CO_2 continue on the current trajectory, nearly ice-free conditions will likely occur by the middle of the century (Jahn et al., 2016; Wang & Overland, 2009, 2012). Trends described in Newton et al. (2017) suggest that transnational ice exchange could continue to expand in the near future, increasing political tensions associated with cross-border contaminant transport (Newton et al., 2016). Here we assess how transnational ice exchange will evolve over the 21st century, and what impact different future emissions scenarios may have on these projections.

Sea ice acts as a transport medium for materials such as dust, aerosol deposits, sediments, organic matter, macro-nutrients, freshwater, and biological communities growing at the bottom of the ice (Eicken et al., 2000; Eicken, 2004; Melnikov et al., 2002; Newton et al., 2013; Nürnberg et al., 1994). Transport of ice algae and sediments by sea ice has been shown to favor ice-associated phytoplankton blooms when the ice melts in the summer, critically impacting the food web structure (Boetius et al., 2013; Fernández-Méndez et al., 2015; Gradinger et al., 2009; Jin et al., 2007; Olsen et al., 2017). As industrialization of the Arctic continues to expand due to easier marine access, anthropogenic pollutants (e.g., mercury, lead, black carbon, oil, microplastics) may also be transported by sea ice over long distances from where they first enter the ocean (AMAP, 2011, 2015; Blanken et al., 2017; Obbard et al., 2014; Peeken et al., 2018; Pfirman et al., 1995, 1997; Shevchenko et al., 2016; Varotsos & Krapivin, 2018; Venkatesh et al., 1990). This makes assessment of risk, attribution of responsibility for environmental and ecological consequences, as well as containment, recovery, and cleaning operations of contaminants very difficult if not impossible (Glickson et al., 2014; Newton et al., 2016; Peterson et al., 2003; Post et al., 2009; Sørstrøm et al., 2010; Wilkinson et al., 2017).

To explore the connections between future changes in Arctic sea ice and emerging political issues related to long-distance rafting of material, we frame our analysis in the context of exclusive economic zones (EEZs; Flanders Marine Institute, 2018) of the Arctic states (Figure 1). This builds on the work by Newton et al. (2017), who used satellite-derived sea ice drifts and analyzed transnational ice transport and change from the years pre to post-2000. An exclusive economic zone is a sea zone over which a state has special rights regarding the exploration and use of marine resources, including energy production. EEZs extend 200 nautical miles from the coastline, as prescribed by the United Nations Convention on the Law of the Sea (Nordquist, 2011). There are five Arctic littoral states: Canada, the United States, Russia, Norway (including the Svalbard archipelago and the Jan Mayen island) and Denmark (Greenland). We also consider Iceland as part of our analysis since it receives sea ice exported from the Arctic Ocean through Fram Strait. We define the Central Arctic (CNT) as the region in the middle of the Arctic Ocean over which no country has exclusive economic rights.

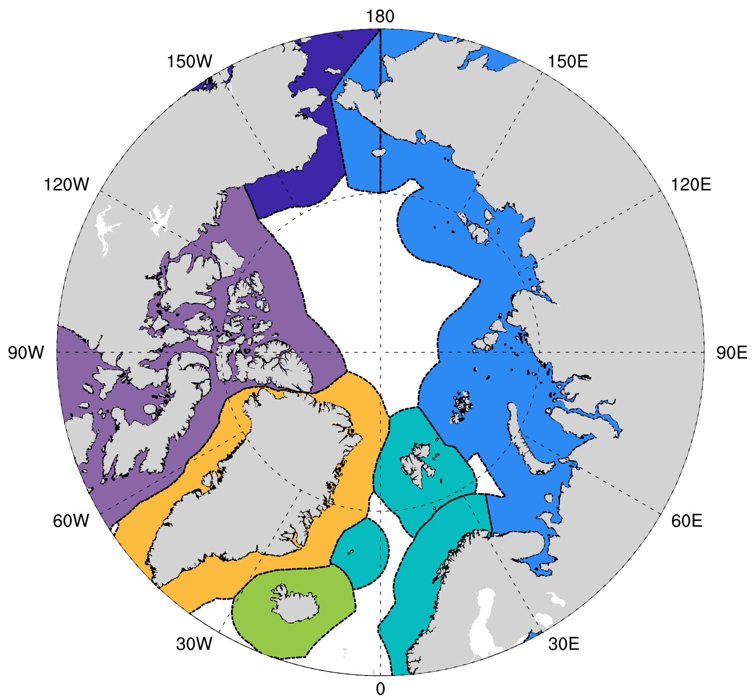

Figure 1. Map of the exclusive economic zones (EEZs) of the Arctic based on the definition from the United Nations Convention on the Law of the Sea (Nordquist, 2011): Canada [*purple*], the United States [*dark blue*], Russia [*light blue*], Norway [*turquoise*], Iceland [*green*] and Greenland [*orange*]. The region in the middle of the Arctic Ocean that is not included within an EEZ is referred to as the Central Arctic (CNT) for the context of this study.

2 Methods

2.1 Community Earth System Model (CESM)

The CESM1 is a state-of-the-art global Earth System Model characterized by a nominal 1° horizontal resolution in all components (Hurrell et al., 2013). This version of the CESM has been widely used for Arctic sea ice studies and generally performs well in capturing the Arctic mean sea ice state, trend and variability (e.g. Barnhart et al., 2016; DeRepentigny et al., 2016; England et al., 2019; Jahn et al., 2016; Labe et al., 2018; Smith & Jahn, 2019; Swart et al., 2015). Although this study only uses a single Earth System Model, it uses two ensembles from that model, allowing for an assessment of scenario differences while considering internal variability uncertainties. Furthermore, a good representation of present-day sea ice properties has been shown to be critical for future projections of summer sea ice conditions (Massonnet et al., 2012), making the CESM an excellent choice for this type of analysis. Note however that results presented here are closely tied to the simulated atmospheric circulation response to future climate forcing in the Arctic, something that varies across climate models and is still an active area of research (Budikova, 2009; Zappa et al., 2018).

To investigate the impact of different future emissions scenarios on the projections of ice exchange between the different EEZs of the Arctic, we use two ensembles of the fully-coupled climate simulations from the CESM1. The CESM Large Ensemble (CESM-LE; Kay et al., 2015) includes 40 individual ensemble members that differ only by round-off level differences in the initial air temperature field (order of 10^{-14} K). These large ensemble simulations follow the historical forcing from 1920 to 2005 and the business-as-usual Representative Concentration Pathway 8.5 (RCP8.5; Jones et al., 2013) emissions scenario from 2006 to 2100 (Figure 2a,b). We also use the CESM ensemble simulations following the 2°C target low warming scenario (CESM-LW; Sanderson et al., 2017). These 2°C target low warming simulations, along with similar experiments using a target of 1.5°C and an overshoot scenario that temporarily exceeds 1.5°C, were designed to inform assessment of impacts at 1.5 and 2°C above pre-industrial levels following the Paris Intergovernmental Panel on Climate Change (IPCC) Agreement of December 2015 (Sanderson et al., 2017; UNFCCC, 2015). The simulations are branched from the first 11 ensemble members (001-011) of the CESM-LE in 2006, after which they follow an emissions scenario designed so that the multi-year global mean temperatures never exceed 2°C above pre-industrial levels (Figure 2d). Emissions

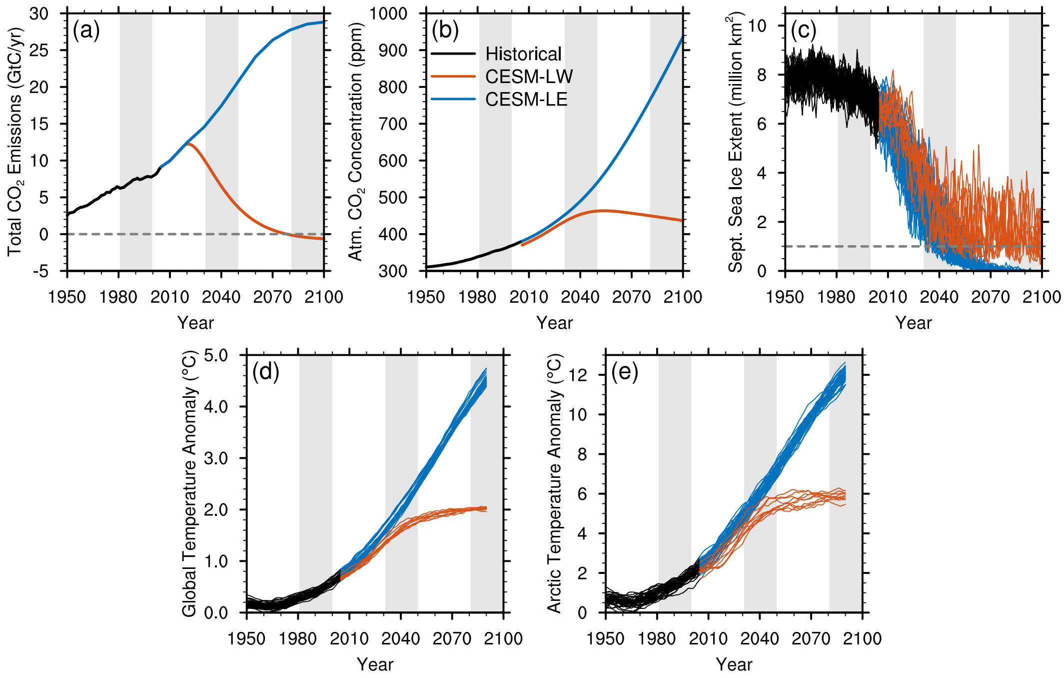

Figure 2. Time evolution of (a) the total CO_2 emissions in GtC/yr, (b) the atmospheric CO_2 concentration in ppm, (c) the September Arctic sea ice extent in million km^2 for all ensemble members with the threshold for a nearly ice-free Arctic shown by the grey dashed line, (d) the 20-year running mean annual-mean global temperature anomalies for all ensemble members (relative to pre-industrial levels, taken as 1850–1920 here) and (e) the 20-year running mean annual-mean Arctic temperature anomalies for all ensemble members. All panels cover the historical period of the CESM-LE [*black*], the future RCP8.5 scenario of the CESM-LE [*blue*] and the future low warming scenario of the CESM-LW [*orange*]. Note the different range of the y-axis for (d) the global temperature anomalies and (e) the Arctic temperature anomalies. The grey shaded areas highlight the three different time periods our analysis focuses on. (Adapted from Figure S.1 of Jahn, 2018).

follow the RCP8.5 scenario from 2006 to 2017, after which they start declining rapidly (Figure 2a), such that emissions in 2042 are half of the 2017 levels (Sanderson et al., 2017). This low warming scenario requires a negative emissions phase in order to stay below the 2°C warming target, with combined fossil fuel and land use carbon emissions crossing net zero in 2078 (Figure 2a). Note that we take the mean of each ensemble to represent the model response to radiative forcing, and the spread about the mean to represent the internal variability within each scenario ensemble.

From all ensemble simulations, we use the u and v components of the sea ice velocity field as well as sea ice concentration (*aice*), at a monthly time resolution. Each variable is interpolated onto the 25 km Equal-Area Scalable Earth Grid (EASE-Grid; Brodzik et al., 2012) in order to conserve sea ice area during the tracking process (see section 2.2 for more details on the ice tracking system). While the CESM-LE also provides sea ice concentration at a daily time resolution for the entire length of the simulation, the u and v components of the sea ice velocity field are only available at a 6-hourly time resolution for three periods varying from 10 to 15 years between 1920 and 2100. In addition, the CESM-LW only provides these variables available at a monthly resolution, which does not allow for an analysis at a higher temporal resolution for this scenario. The effect of the time resolution on our analysis has been tested by comparing weekly and monthly averages for the CESM-LE, and the results show no major change to the conclusions presented here (see Figures S1 and S2 in the supporting information for more details).

In this study, the CESM analysis is separated into three time periods of 20 years, separated equally from the end of the 20$^{\text{th}}$ century to the end of the 21$^{\text{st}}$ century: (1) 1981 to 2000, (2) 2031 to 2050 and (3) 2081 to 2100. Each period captures a different regime of the transition toward a seasonally ice-free Arctic (see Figures 2c and 3 for context), allowing us to assess the projected evolution of sea ice exchange:

1981–2000 Representative of the state of the Arctic at the end of the 20$^{\text{th}}$ century, before the start of the observed series of record low minima in September sea ice extent of under six million km^2 (can be compared to the pre-2000 period used in Newton et al., 2017);

2031–2050 Representative of a thin and dynamic ice pack, mostly consisting of first-year ice except for the region north of Greenland and the Canadian Arctic Archipelago (Figure 3b,c);

2081–2100 Representative of a fully seasonal ice cover for the CESM-LE, with a nearly ice-free Arctic over three to five months for all 40 ensemble members (Figure 2c), and nearly ice-free summers for a maximum of one month every few years for the CESM-LW due to less sea ice loss (Jahn, 2018).

In order to provide an assessment of the performance of the CESM in simulating sea ice transport between EEZs, we also analyze the CESM-LE over the 20-year period between 1989 and 2008 and compare it with observational data (section S2 in the supporting infor-

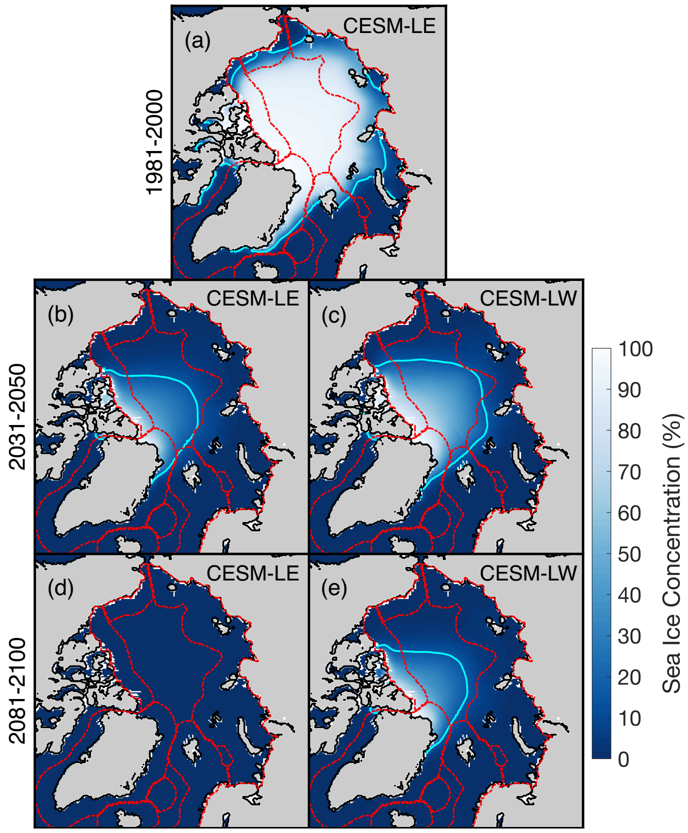

Figure 3. Average September sea ice concentration for the CESM-LE over the period of (a) 1981–2000 as well as for (b,d) the CESM-LE and (c,e) the CESM-LW over the periods of (b,c) 2031–2050 and (d,e) 2081–2100. The borders of the EEZs are indicated by red lines. The cyan line shows the 15% sea ice concentration contour.

mation). This period is slightly shifted compared to the first period of the CESM analysis due to a low bias in satellite-derived drift vectors prior to 1989 (section S1 in the supporting information). We use data from the National Snow and Ice Data Center's (NSIDC) Polar Pathfinder project (Tschudi et al., 2016) and the National Oceanic and Atmospheric Administration (NOAA)/NSIDC Climate Data Record (Meier et al., 2017; Peng et al., 2013). We find that the exchange of transnational ice between the different EEZs of the Arctic simulated by the CESM-LE over the period of 1989–2008 is in good general agreement with observations. The small differences between the CESM-LE and observations can be attributed to a bias in the simulated atmospheric circulation over the Arctic during the ice-covered season and the resulting sea ice circulation anomalies (see section S2 for more details).

2.2 Sea Ice Tracking Utility (SITU)

We use a Lagrangian approach to better understand the potential connections between the Arctic states through the sea ice they exchange. To that end, we use a Lagrangian tracking software called the Sea Ice Tracking Utility (SITU, `http://icemotion.labs.nsidc.org/SITU/`), formerly known as the Lagrangian Ice Tracking System (LITS; DeRepentigny et al., 2016; Williams et al., 2016; Brunette et al., 2019), that tracks ice floes from their formation location to where they ultimately melt. This offline approach to Lagrangian modeling uses saved output from preexisting runs of the model and requires significantly less computational resources compared to the transport of online tracers. SITU allows us to obtain a quantitative assessment of the evolution of ice motion by looking at the exchange of sea ice between the EEZs of different Arctic states and how these patterns are predicted to change in the future. This software has been successfully used to track ice floes forward or backward in time (DeRepentigny et al., 2016; Newton et al., 2017; Williams et al., 2016) and is based on a similar approach that has been widely used to track ice age over several years (Fowler et al., 2004; Maslanik et al., 2007; Pfirman et al., 2004; Rigor & Wallace, 2004).

In the present analysis, SITU is used to track ice area. This requires all of the output variables to be interpolated to an equal-area grid for the area to be conserved during the tracking process. Note that this method does not aim to fully capture sea ice physics, as it does not track ice volume and uses data at a 25 km resolution. Nonetheless, tracking independent parcels of ice area provides some information on the effect of sea ice convergence, as SITU allows for multiple tracked ice parcels to stack up in the case of convergent flow. This approximates a rise in ice thickness through ridging by increasing the number of tracked areal parcels of ice over a specific location. For this study, we analyze transnational ice exchange in terms of areal flux rather than the areal flux divided by the area covered by each EEZ, as this is more representative of the potential risk for ice-rafted contaminant transport.

First, for every month considered within the analysis, the location of newly formed ice floes is identified. A newly ice-covered grid cell can either be the product of ice formation (freezing) or advection of ice from a nearby location. In order to dissociate the thermodynamic signal from the dynamic signal, we select all grid points along the ice edge (defined as the 15% ice concentration contour), track them forward in time for one month using the sea ice velocity at each grid point along the ice edge, and compare the result with the sea ice edge of the following month. Every grid cell outside of the tracked ice edge that was not covered by ice initially but is ice covered the following month is then considered a new ice parcel (referred to hereafter as an ice formation event). Next, all ice formation events are fed to SITU, which advects each newly formed ice parcel forward in time with a monthly resolution until it ultimately melts, creating a record of ice tracks. An ice parcel is considered to have melted when it is advected to a location that is ice free when compared with the ice concentration field of that month. Melt (and formation explained above) is defined using a sea ice concentration threshold of 15%. The transition between ice and open water is usually abrupt and our results show no sensitivity to the exact choice of cut-off value (not shown).

Using time-averaged velocities (monthly averages in the case of the analysis presented here) can result in floes being advected over land (either an island or the continent) by SITU instead of piling up along the coast. To avoid unrealistic loss of ice floes over land within SITU, we move the affected parcels back to the last ocean grid cell they crossed prior to reaching land, following a linear trajectory between their initial position and their position after one time step. These parcels continue to be tracked normally, subject to the dynamics of their new location as if they had simply piled up along the coast.

In what follows, we analyze what we refer to as "transnational" sea ice, ice that leaves the EEZ in which it formed, as distinguished from "domestic" ice that melts in the same EEZ where it formed. We also refer to the fraction of transnational ice exchange, defined as the ratio of the areal flux of transnational sea ice to the total areal flux of sea ice, transnational and domestic combined.

3 Results

3.1 Increase in Transnational Ice Exchange

Over the last 20 years of the 20$^{\text{th}}$ century, Russia dominates in terms of formation of transnational ice (74.8% of the total areal flux of transnational ice originates from Russia) and the majority of transnational Russian ice gets exported to Norway (Figure 4a), in general agreement with observations (see section S2 in the supporting information or Newton et al., 2017). Using SITU, we find an increase in the area of ice formed each year from 1.4 million km^2/yr in 1981–2000 for the CESM-LE to between 4.6 and 5.3 million km^2/yr in 2031–2050

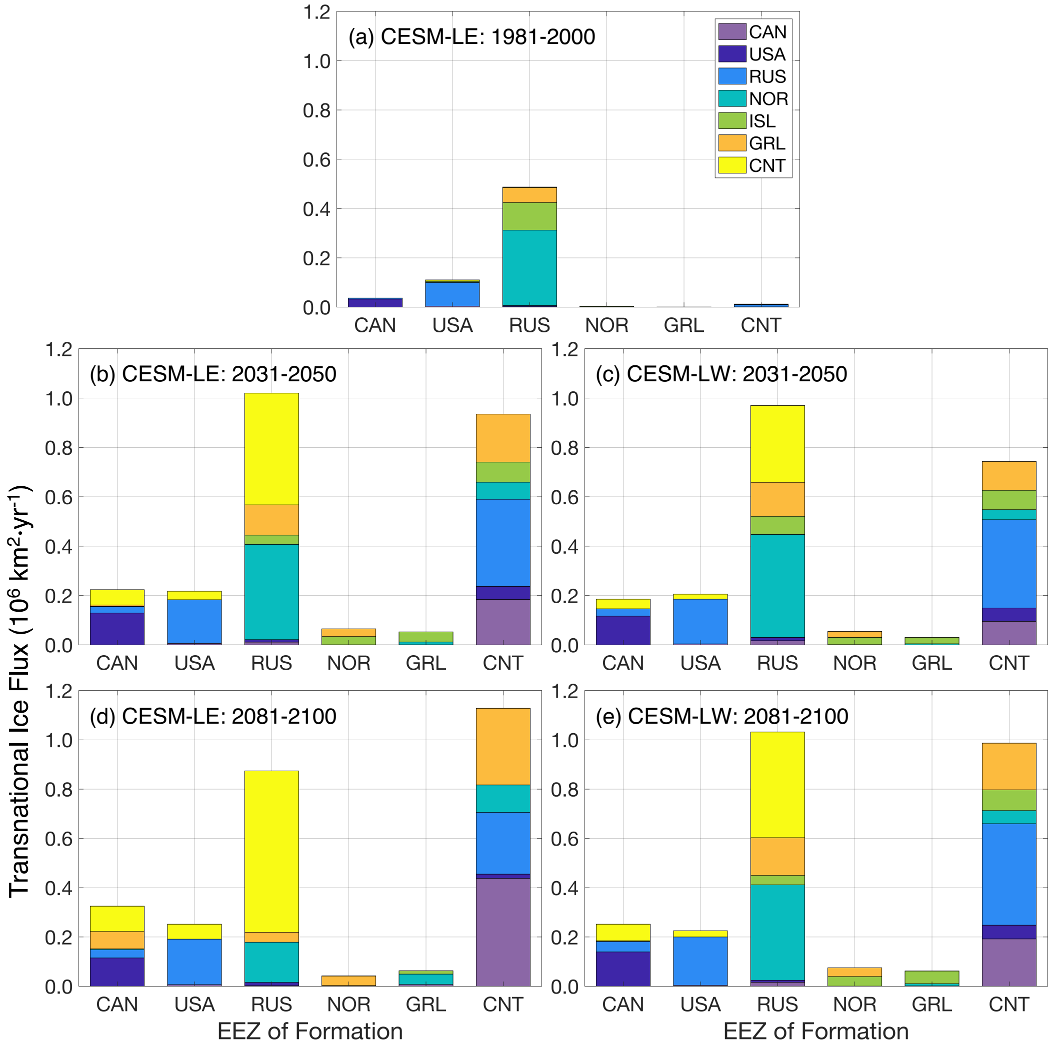

Figure 4. Annual mean average areal flux of transnational ice for the CESM-LE over the period of 1981–2000 [*top* - (a)] and for the CESM-LE [*left* - (b,d)] and the CESM-LW [*right* - (c,e)] over the periods of 2031–2050 [*middle* - (b,c)] and 2081–2100 [*bottom* - (d,e)]. The height of each colored portion within one bar represents the annual mean areal flux of ice between the EEZ of formation (x-axis) and the EEZ of melt (color). Note that domestic ice is not included in this figure in order to focus on the features of transnational ice exchange. The average amount of ice area exchanged between all EEZs, including domestic ice, for both experiments as well as a statistical assessment of the pathways that are significantly different between the CESM-LE and the CESM-LW can be found in Tables S1 and S2 in the supporting information.

for the CESM-LW and the CESM-LE, respectively. This large increase in ice formation is accompanied by an increase in the amount of transnational ice exchanged between the different EEZs by mid-century. In fact, the total average areal flux of transnational ice in the Arctic increases by 252% for the CESM-LE and 204% for the CESM-LW between the periods of 1981–2000 and 2031–2050 (Figure 4b,c).

The main reason for this large increase in transnational ice flux from 1981–2000 to 2031–2050 is the poleward expansion of the seasonal ice zone (SIZ), defined as the area between the minimum and maximum sea ice extents, due to a continued rise in simulated Arctic temperatures (Figure 2e). By mid-century, under both scenarios, the area of annual sea ice formation expands from the peripheral seas to almost the entire Arctic Ocean (Figure 5a-f). Over the period of 2031–2050, the spatial differences in ice formation between the CESM-LE and the CESM-LW are small (Figure 5c-f), with slightly more extensive ice formation over the Central Arctic for the CESM-LE in the fall due to lower average September sea ice extent (Figures 2c and 3b,c). By mid-century, only the region north of Greenland and the Canadian Arctic Archipelago survives the summer melt (Figure 6c-f) and is reliably ice covered in September (Figure 3b,c). The increase in the area of the SIZ by 2031–2050 allows for more ice to be formed each year and to melt in a different EEZ than the one where it initially formed.

Another key feature of the future projections of sea ice transport is that by mid-century, Russia and the Central Arctic strongly dominate the exchange of transnational ice in the Arctic. The areal flux of transnational ice originating from Russia doubles by mid-century, and for the Central Arctic it increases from less than 13 thousand km^2/yr to just below one million km^2/yr for the CESM-LE (Figure 4a,b). The increase in Russian transnational ice is predicted to occur as the whole area of the Russian EEZ becomes a source and a sink of sea ice in 2031–2050 (Figures 5c,e and 6c,e), whereas formation and melt is limited to its coastal regions in 1981–2000 (Figures 5a and 6a). This larger area of sea ice loss in the summer months could potentially promote economic activities in the Russian EEZ and increase the risk of ice-rafted contaminant transport (Newton et al., 2016; Pfirman et al., 1995). As for the Central Arctic, it accounts for 37.2% of the total formation of transnational ice area in 2031–2050 for the CESM-LE (Figure 4b), up from less than 2% in 1981–2000 (Figure 4a). In addition to becoming an important source region for transnational ice, the Central Arctic also becomes an important sink, with the percentage of transnational ice melting in this region increasing from 1.1% in 1981–2000 to 21.8% in 2031–2050 for the CESM-LE (Figure 4a,b). This can be partly explained by the fact that ice formation/melt is present over most of the Central Arctic by mid-century (Figures 5c,e and 6c,e), whereas there is

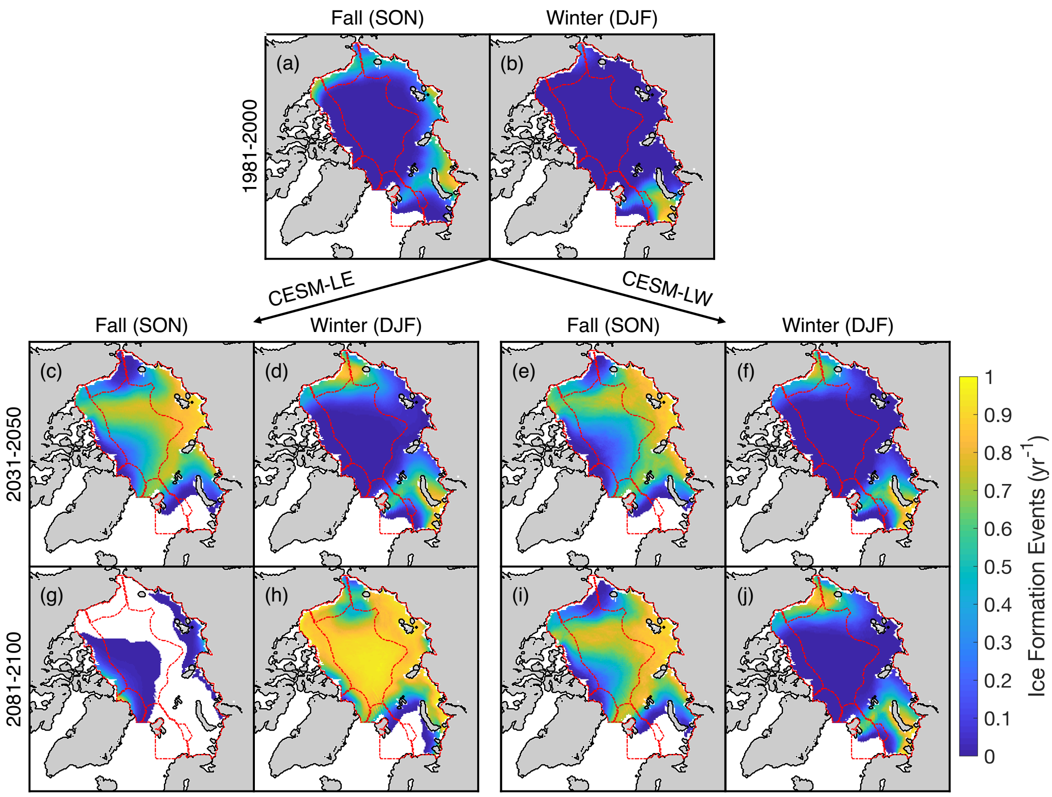

Figure 5. Average number of ice formation events per year in fall (SON) and winter (DJF) for the CESM-LE over the period of 1981–2000 [*top* - (a,b)] and for the CESM-LE [*left* - (c,d,g,h)] and the CESM-LW [*right* - (e,f,i,j)] over the periods of 2031–2050 [*middle* - (c-f)] and 2081–2100 [*bottom* - (g-j)]. Only grid cells that are ice covered for at least one month during the specified season and time period and for a least one ensemble member are colored. The borders of the EEZs are indicated by red lines. Only ice floes that formed and melted between the specified time periods are considered.

little to no ice formation/melt over that region in 1981–2000 (Figures 5a and 6a). The large contribution of Russia and the Central Arctic to the exchange of transnational ice is not surprising considering the surface area covered by these two EEZs. Note however that it is the total areal flux of transnational ice, not the flux per unit area, that best represent the extent of potential ice-rafted contaminant transport (Newton et al., 2017).

3.2 Impact of the Future Emissions Scenario

The difference in the response of sea ice transport to the two future emissions scenarios becomes more apparent toward the end of the 21st century. Over the last 20 years of

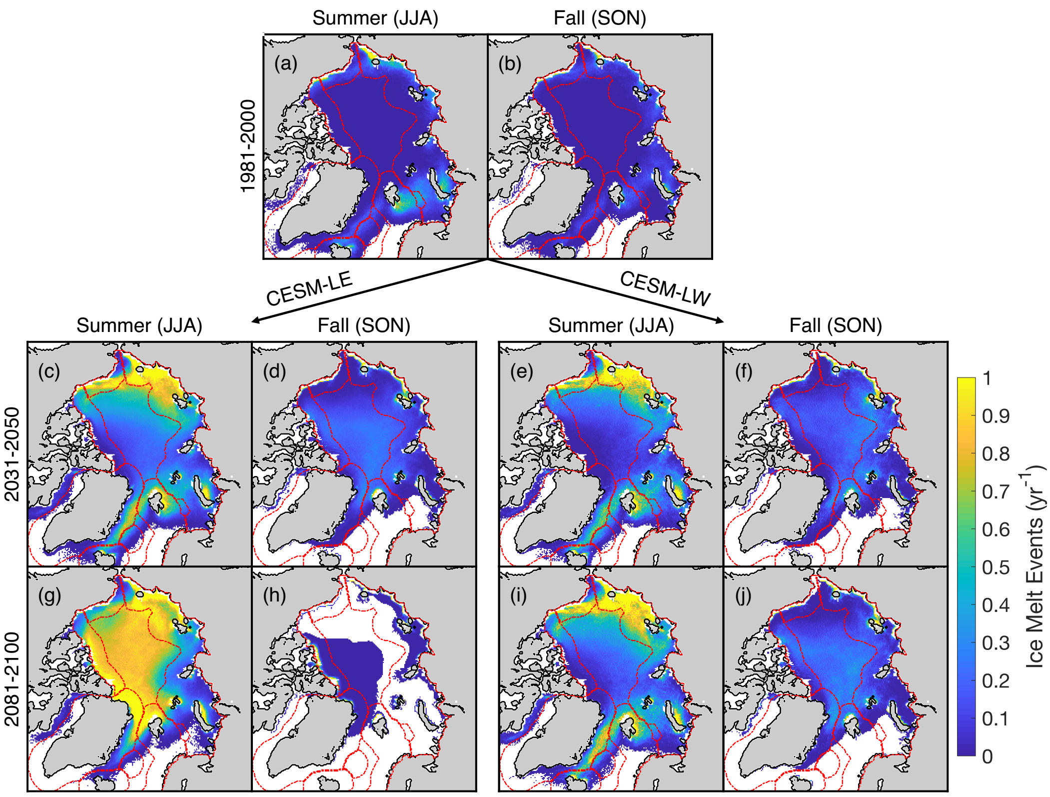

Figure 6. As in Figure 5, but for the average number of ice melt events per year in summer (JJA) and fall (SON).

the 20$^{\text{th}}$ century, ice formation and melt peak in October and August, respectively (Figure 7a,b). There is a large increase in the total annual amount of areal ice formation and melt by 2031–2050, with the peak in ice formation shifting from October to November for both future emissions scenarios (Figure 7c,d). Large differences in the ensemble mean ice formation and melt between the CESM-LE and the CESM-LW are projected by 2081–2100. The ensemble mean represents the best estimate of the forced response to the future emissions scenario, while the spread about the mean is used to assess the confidence of that forced response based on the internal variability of the climate system. The ensemble mean of the CESM-LE has ice formation and melt peak in January and July respectively by the end of the century, compared to November and August for the CESM-LW (Figure 7e,f), much more similar to present-day conditions. In addition, the annual cycles of ice formation and melt for the CESM-LE and the CESM-LW are statistically different at the 95% confidence level in 2081–2100 during all months of the growing and melting seasons, respectively. Compared to the period of 1981–2000, the length of the ice-covered season (defined here as the number

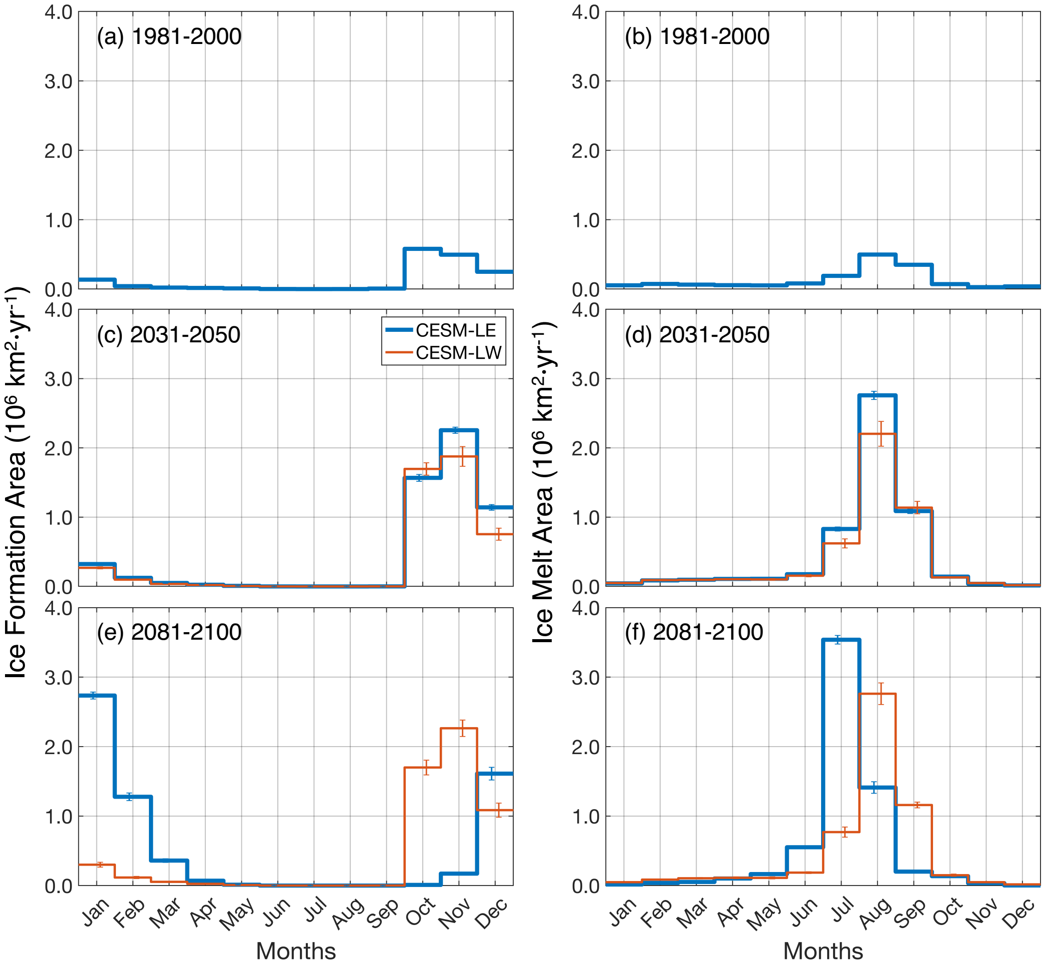

Figure 7. Annual cycle of areal ice formation [*left*] and melt [*right*] for the periods of 1981–2000 (a,b), 2031–2050 (c,d) and 2081–2100 (e,f) in the CESM-LE [*blue*] and the CESM-LW [*orange*]. The error bars show the 95% confidence intervals of the 20-year averaged ice formation/melt area for each month across the 40 ensemble members of the CESM-LE and the 11 ensemble members of the CESM-LW. Only ice floes that formed and melted between the specified time periods are considered.

of months from the peak in ice formation to the peak in ice melt) is predicted to decrease by one month for the CESM-LW and four months for the CESM-LE by 2081–2100 when looking at the forced signal. By the end of the 21st century, earlier ice formation as well as later melt in the CESM-LW gives more time for ice floes to transit the Arctic before the start of the melt season compared to the CESM-LE, which has a shorter ice-covered season. In turn, longer travel times allow for larger traveled distances, promoting transnational ice exchange in the CESM-LW compared to the CESM-LE. Note that the annual formation and melt cycles of the CESM-LW over the period of 2081–2100 are very similar to the ones of the CESM-LE in 2031–2050, pointing to a stabilization of the sea ice response under the low emissions scenario around mid-century climate when atmospheric CO_2 starts to slowly decline (Figure 2b).

Spatial differences in ice formation and melt between the two future emissions scenarios also manifest at the end of the 21st century. By 2081–2100, the ice formation season shifts from fall (SON) to winter (DJF) everywhere in the Arctic for the CESM-LE, as freezing starts and ends later in the year (Figures 5g,h and 7e; see also Smith & Jahn, 2019). For the CESM-LW on the other hand, most of ice formation still occurs in the fall (Figures 5i and 7e), with the exception of parts of the Barents, Kara, Beaufort and Chukchi Seas (Figure 5j). Moreover, melt occurs over the whole Arctic basin in summer only for the CESM-LE (Figure 6g,h), which simulates a nearly ice-free Arctic for several months each year by the late 21st century (see also Jahn, 2018). For the CESM-LW, melt still occurs in the fall north of Greenland and the Canadian Arctic Archipelago and into the Central Arctic in the late 21st century (Figure 6j), similar to mid-century conditions in the CESM-LE (Figure 6d). As a result, there is a longer portion of the year when the Arctic is fully ice covered in the CESM-LW, allowing more time for ice floes to move around and increasing the amount of ice exchanged between the different EEZs.

The CESM also projects a large reduction in the average amount of time necessary for sea ice to transit from one EEZ to another by 2031–2050, especially for long pathways that are characterized by an average transit time of more than two years in 1981–2000 (Figure 8). This decrease in transit times is related to the poleward expansion of the SIZ, which acts to melt a larger area of ice each summer and greatly reduce the number of multi-year transit pathways, in combination with an increase in ice drift speed, especially in the winter months (not shown; see also Tandon et al., 2018). The increase in ice drift speed is mainly associated with a decrease in ice thickness as we find no significant change in the average wind speed over the Arctic throughout the 21st century (not shown). By 2081–2100, all exchange pathways have average transit times of less than one year for the CESM-LE (Figure 8). This is the result of a seasonal ice cover over the whole Arctic basin, which prevents the formation of multi-year ice in all of the 40 ensemble members and does not allow for transit times longer than one year. On the other hand, the CESM-LW shows transit times in 2081–2100 that are similar to those of the CESM-LE in 2031–2050 (Figure 8), again pointing to a stabilization of the sea ice response to the reduced atmospheric CO_2

concentration in the CESM-LW scenario toward the end of the century (Figure 2b). Note that transit times for all exchange pathways for the CESM-LW by 2081–2100 are statistically different from 1981–2000 transit times at the 95% confidence level, except for ice forming in the Central Arctic and melting in the United States (Figure 8). Moreover, for the period of 2081–2100, all transit time differences between the CESM-LE and the CESM-LW are statistically significant.

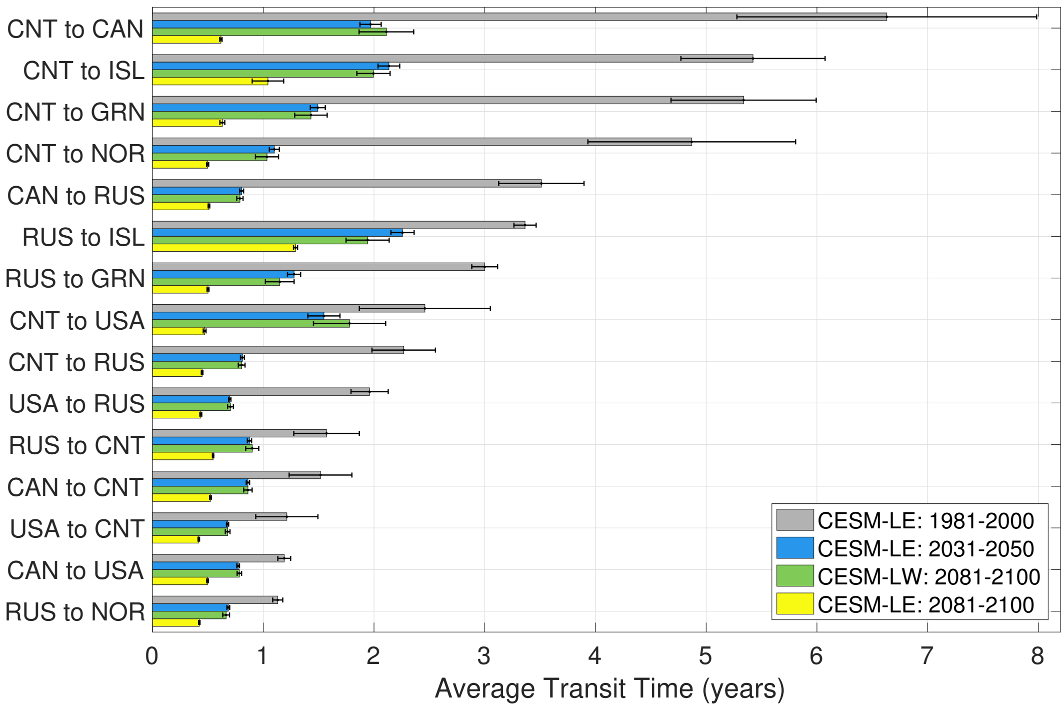

Figure 8. Average transit time in years for the 15 pathways exchanging the largest areal flux of transnational ice throughout all three time periods and both experiments. The error bars show the 95% confidence bounds of the 20-year averaged transit time for the 40 ensemble members of the CESM-LE and the 11 ensemble members of the CESM-LW.

As the melt season is projected to get longer and average transit times shorten to less than one year for the CESM-LE by the end of the 21^{st} century, long-distance ice transport pathways are predicted to diminish in favor of ice exchanged between neighboring EEZs, specifically the ones downstream of each EEZ of formation following the general Arctic sea ice circulation. As a result, the diversity of EEZs of melt for each EEZ of formation is reduced for the CESM-LE compared to the CESM-LW in 2081–2100, especially for Russia and the Central Arctic where the largest amount of transnational ice originates (Figure 4d,e). This implies a continuation in the future of the negative trend in Siberian shelf ice reaching Fram Strait since the beginning of the 21st century recently found by Krumpen et al. (2019). Note that for all exchange pathways over the period of 2081–2100, only the flux of ice from Canada to Russia, from the United States to Russia and from Norway to Greenland (i.e., relatively short-distance downstream fluxes) are not statistically different between the CESM-LE and the CESM-LW at the 95% confidence level. By 2081–2100, consistent nearly ice-free summers in the CESM-LE act to reduce the fraction of transnational ice exchange (as defined in section 2.2), whereas the CESM-LW continues to see an increase. Indeed, the fraction of transnational ice exchange grows from 46% to 48% to 49% for the CESM-LW throughout the three time periods of interest, whereas it initially increases from 46% to 47% between the first two time periods for the CESM-LE, but then reduces to 44% by the end of the 21st century. Note that the fractions of transnational ice exchange are statistically different from each other at the 95% confidence level between the three time periods only for the CESM-LE. It is important to note that even though the fraction of transnational ice exchange decreases for the CESM-LE between 2031–2050 and 2081–2100, the total areal flux of transnational ice increases slightly over the same period. Nonetheless, this result points to the fact that when the Arctic reaches nearly ice-free conditions and the SIZ covers the full Arctic Ocean, increases in the melt season length associated with continuously warmer Arctic temperatures (Figure 2e) will eventually act to reduce the absolute amount of transnational ice exchange, reversing the trend predicted by the CESM-LE over the 21st century.

4 Discussion

In this contribution, we show that as the SIZ expands the amount of sea ice formed each year increases greatly by mid-century, leading to an increase of more than 200% in the area of sea ice exchanged between the different regions of the Arctic. This increase in transnational ice exchange amplifies the potential for ice-rafted contaminant transport, raising environmental risks and accentuating emergent political tensions as the Arctic states are effectively brought into closer contact with each other (Arctic Council, 2009; Emmerson & Lahn, 2012; Newton et al., 2016; Pfirman et al., 1995). A prominent example is the export of ice from Russia to Norway. A heated debate persists in Norway about whether their regulations of offshore drilling, which are some of the most extensive in the world, are sufficient. However, our study indicates that the main risk for Norway in the next few years might be from Russian oil spills, since about 400,000 km^2 of ice transit from the

Russian to the Norwegian EEZ annually by mid-century. In addition, our results show that the trajectory of future greenhouse gases emissions will have a high impact on export of ice from Russia to Norway, as the low emissions scenario predicts a similar amount of ice transit by 2100 as mid-century conditions, compared to a reduction by more than half under the high emissions scenario.

Pollutants of primary concern in the Arctic are organochlorines, heavy metals, radionuclides and oil (Pfirman et al., 1995), which can take years to biodegrade in the Arctic due to the cold Arctic waters (Fingas & Hollebone, 2003). While freezing ejects many dissolved contaminants found in sea water, ice formed in shallow regions (< 50 m) of the Siberian seas has been shown to entrain sediments and organic material (Smedsrud, 2001, 2002) and hence also incorporates associated contaminants. After several years of transport, due to annual surface melting and ablation, a concentrated lag deposit of sediment, organic material and/or contaminants can form on the surface of the ice (Pfirman et al., 1995; Tremblay et al., 2015). Although some contaminants are lost in meltwater runoff, other pollutants are also added from atmospheric deposition of Arctic haze (Octaviani et al., 2015). Furthermore, potential oil spills or shipping accidents can also add contaminants on the ice surface (Fingas & Hollebone, 2003; Glickson et al., 2014; Izumiyama et al., 2004; Venkatesh et al., 1990; Wilkinson et al., 2017). As a result, the majority of ice-rafted pollutants are released when the entire floe melts despite differences in their sources (Pfirman et al., 1995).

Based on our analysis of sea ice transport between the different EEZs of the Arctic, a little more than half of the ice melts in the same EEZ where it formed, meaning that a large part of the contaminants introduced into sea ice will be released within the same EEZ (Newton et al., 2017). However, we find that due to a large increase in the area of sea ice formed every year, the absolute amount of transnational ice exchanged between the different Arctic nations increases by a factor of three between the end of the 20$^{\text{th}}$ century and the middle of the 21$^{\text{st}}$ century. As such, the potential for sea ice to carry contaminants is greatly amplified. The doubling of transnational ice originating from the Russian EEZ by mid-century is of especially high relevance given that most of the Russian EEZ consists of shallow seas where contaminants can be easily incorporated during sea ice formation. In addition, the prospect of undiscovered oil and gas on the Siberian shelves (Bird et al., 2008) and the increase in shipping activities along the Northern Sea Route (Aksenov et al., 2017; Ostreng et al., 2013; Schøyen & Bråthen, 2011; Stephenson et al., 2013) will amplify the risk of pollutants being introduced in these shallow Arctic waters.

The opening of the Central Arctic is also of high significance given the prospect for commercial ships to use the Transpolar Sea Route in order to avoid crossing the EEZ of several Arctic states (Stephenson et al., 2013), increasing the risk of accidental release of contaminants onto sea ice. The lack of risk management policies regulating the release of pollutants in these international waters combined with a short operational season, large distances to ports and other infrastructure, and the generally challenging Arctic environment will likely make this region very vulnerable to long-term contamination. Compared to the Russian shelf seas, the Central Arctic covers mostly deep waters, so contamination of surface waters by oil spills and atmospheric deposition of black carbon and other emissions are likely the main concerns for this region.

5 Conclusions

In this study, we have addressed the question: "How will the exchange of transnational sea ice evolve in the future?", using two ensemble experiments of the CESM that range from 2°C to over 4°C of global warming by 2100. We find a large increase in the area of transnational ice exchanged in the Arctic throughout the 21^{st} century, continuing the trend reported by Newton et al. (2017) over the observational period. The CESM captures the exchange of transnational ice in the Arctic well when compared to satellite observations over the 1990s and 2000s, with a few disagreements that can be attributed to a bias in the simulated atmospheric circulation over the Arctic during the ice-covered season. When looking at future projections, we found that the CESM projects the largest increase in the amount of transnational ice exchange between the end of the 20^{th} century and the middle of the 21^{st} century, under both forcing scenarios. This increase is associated with the expansion of the SIZ from the peripheral seas toward the middle of the Arctic Ocean, as global and Arctic temperatures continue to rise. The expansion of the SIZ in 2031–2050 allows for more ice to be formed each year which, combined with a decrease in the average time it takes for an ice floe to go from one EEZ to another, acts to promote transnational ice exchange in the Arctic.

The increase in transnational ice exchange by mid-century and until 2100 is not uniform everywhere in the Arctic, but is dominated by Russia and the Central Arctic as they include a large fraction of the SIZ. We find that by 2031–2050, 78% of transnational ice originated from these two regions, while also accounting for 44% of the melt of transnational ice in the CESM-LE. Long exchange pathways that are characterized by an average transit time of more than two years in 1981–2000 see a large reduction in travel time as less ice transits along these routes, with all pathways exchanging ice in two years or less by mid-century. We also find that differences in the forced sea ice response to a high versus low emissions scenario become most apparent toward the end of the 21st century. By 2081–2100, the CESM-LW has a longer ice-covered period than the CESM-LE, due to earlier ice formation and later ice melt. This gives ice floes more time to travel from one EEZ to another before the start of the melt season, promoting transnational ice exchange in the CESM-LW. Indeed, we find that all exchange pathways have average transit times of one to two years for the CESM-LW that persist through 2081–2100, similar to mid-century transit times for both scenarios. By comparison, average transit times are all less than one year for the CESM-LE by 2081–2100 due to consistent nearly ice-free summers of three to five months for all 40 ensemble members (Jahn, 2018).

Ice transport along long-distance pathways are predicted to diminish in favor of ice exchange between neighboring EEZs by the end of the 21st century under the high emissions scenario, specifically shifting to the EEZs downstream of each EEZ of formation. This is the result of a projected lengthening of the melt season, which decreases average transit times to less than one year for the CESM-LE, continuing the trend recently reported by Krumpen et al. (2019) and Newton et al. (2017). In fact, the CESM-LE shows a decrease in the fraction of transnational ice exchange between the periods of 2031–2050 and 2081–2100, whereas the CESM-LW continues to see an increase. Even though the total areal flux of transnational ice continues to increase slightly for the CESM-LE over the same time window, the decline of the fraction of transnational ice exchange has important implications for transnational ice exchange after 2100. A previous version of the CESM, the Community Climate System Model Version 4 (CCSM4), RCP8.5 simulations and their extension to 2300 show that September ice extent will not recover under this business-as-usual scenario, and March ice extent will continue to decrease and reach nearly ice-free conditions toward the middle of the 23rd century (Jahn & Holland, 2013). Our results suggest that the predicted increase in melt season length associated with continuously warmer Arctic temperatures would eventually act to reduce the total amount of transnational ice exchanged between the EEZs of the Arctic, reversing the trend predicted by the CESM over the 21st century for all scenarios.

To conclude, our study shows that the characteristics of transnational ice exchange will change dramatically over the 21st century, even under a low warming scenario. As a result, the potential for ice-rafted contaminant transport across EEZs will increase greatly in the next few decades. Given the associated societal risks, our results suggest that in order to support risk management strategies for ice-rafted contaminants, more detailed modeling should be undertaken in the future, to simulate specific pollutants. Such a model would have to include exchange and transport of multiple tracers with a surface deposition source for atmospheric aerosols and particulates, sedimentary inclusion for sea ice formed in shallow waters, and a potential for ice-trapped oil from open-water spills.

Acknowledgments

P. DeRepentigny acknowledges the support of the Natural Sciences and Engineering Council of Canada (NSERC), the Fond de recherche du Québec – Nature et Technologies (FRQNT) and the Canadian Meteorological and Oceanographic Society (CMOS) through PhD scholarships. P. DeRepentigny is also supported by NSERC Discovery Program funds awarded to L. B. Tremblay, NSF-OPP grant 1504348 (PI: A. Jahn, co-PIs: L. B. Tremblay and M. M. Holland), and A. Jahn's start-up funds from the University of Colorado Boulder. A. Jahn acknowledges support from NSF-OPP grant 1504348 and start-up funds from the University of Colorado Boulder. L. B. Tremblay is grateful for the financial support of the NSERC Discovery Program and the MEOPAR grant "Forecasting Regional Arctic Sea Ice from a Month to Seasons". This work is a contribution to the Canadian Sea Ice and Snow Evolution (CanSISE) Network funded by the NSERC Climate Change and Atmospheric Research program. R. Newton's effort on this project has been supported by the National Science Foundation grants NSF-OCE 14-36666 (Arctic GEOTRACES) and NSF-PLR 15-04404 (Dynamics of Freshwater Components). S. Pfirman's contribution has been supported by the Arizona State University. This project is part of the grant "A Lagrangian approach to emerging dynamics of the marginal ice zone", lead PI: L. B. Tremblay, co-PIs: S. Pfirman and R. Newton, ONR N00014-11-1-0977, 2011-2016.

We acknowledge the CESM Large Ensemble Community Project and the CESM Low Warming Ensemble Project. The CESM project is supported primarily by the National Science Foundation (NSF). Computing and data storage resources, including the Cheyenne supercomputer (doi:10.5065/D6RX99HX), were provided by the Computational and Information Systems Laboratory (CISL) at NCAR. Model output for the CESM-LE and the CESM-LW is publicly available on the Earth System Grid website at `www.earthsystemgrid.org`. The Polar Pathfinder data set is publicly available on the NSIDC website at `http://`

`nsidc.org/data/NSIDC-0116`. The Climate Data Record product is publicly available on the NSIDC website at `http://nsidc.org/data/G02202`. Shapefiles of maritime boundaries and EEZs are publicly available at `http://http://www.marineregions.org/`.

L. B. Tremblay, S. Pfirman and R. Newton conceived the overall research question, starting from the work of S. Pfirman and W. Haxby (deceased) on Lagrangian sea ice tracking. A. Jahn suggested including the low warming scenario in the analysis. L. B. Tremblay, R. Newton and P. DeRepentigny implemented the Sea Ice Tracking Utility (SITU) and computational framework. P. DeRepentigny carried out the experiments and performed the analysis under the supervision of L. B. Tremblay and A. Jahn. P. DeRepentigny took the lead in writing the manuscript. All authors provided critical feedback and collaborated in shaping the research, analysis and final version of the manuscript. We acknowledge comments on an earlier draft by Dr. Clara Deser, Dr. Marika M. Holland, Dr. Jennifer E. Kay and Dr. Walt N. Meier.

References

Aksenov, Y., Popova, E. E., Yool, A., Nurser, A. G., Williams, T. D., Bertino, L., & Bergh, J. (2017). On the future navigability of Arctic sea routes: High-resolution projections of the Arctic Ocean and sea ice. *Marine Policy*, *75*, 300–317. doi: https://doi.org/10.1016/j.marpol.2015.12.027

AMAP. (2011). *AMAP Assessment 2011: Mercury in the Arctic* (Tech. Rep.). Oslo, Norway: Arctic Monitoring and Assessment Programme (AMAP). (Available at: `https://www.amap.no/documents/doc/amap-assessment-2011-mercury-in-the-arctic/90`)

AMAP. (2015). *AMAP Assessment 2015: Black carbon and ozone as Arctic climate forcers* (Tech. Rep.). Oslo, Norway: Arctic Monitoring and Assessment Programme (AMAP). (Available at: `https://www.amap.no/documents/doc/amap-assessment-2015-black-carbon-and-ozone-as-arctic-climate-forcers/1299`)

Arctic Council. (2009). *Arctic Marine Shipping Assessment 2009 Report* (Tech. Rep.). Oslo, Norway: Arctic Council Norwegian Chairmanship. (Available at: `https://oaarchive.arctic-council.org/handle/11374/54`)

Barnhart, K. R., Miller, C. R., Overeem, I., & Kay, J. E. (2016). Mapping the future expansion of Arctic open water. *Nature Climate Change*, *6*(3), 280. doi: https://doi.org/10.1038/nclimate2848

Bird, K. J., Charpentier, R. R., Gautier, D. L., Houseknecht, D. W., Klett, T. R., Pitman,

J. K., … Wandrey, C. R. (2008). *Circum-Arctic resource appraisal: Estimates of undiscovered oil and gas north of the Arctic Circle* (Tech. Rep.). U.S. Geological Survey. doi: https://doi.org/10.3133/fs20083049

Blanken, H., Tremblay, L. B., Gaskin, S., & Slavin, A. (2017). Modelling the long-term evolution of worst-case Arctic oil spills. *Marine Pollution Bulletin*, *116*(1-2), 315–331. doi: https://doi.org/10.1016/j.marpolbul.2016.12.070

Boetius, A., Albrecht, S., Bakker, K., Bienhold, C., Felden, J., Fernández-Méndez, M., … others (2013). Export of algal biomass from the melting Arctic sea ice. *Science*, *339*(6126), 1430–1432. doi: https://doi.org/10.1126/science.1231346

Brodzik, M. J., Billingsley, B., Haran, T., Raup, B., & Savoie, M. H. (2012). EASE-Grid 2.0: Incremental but significant improvements for Earth-gridded data sets. *ISPRS International Journal of Geo-Information*, *1*(1), 32–45. doi: https://doi.org/10.3390/ijgi1010032

Brunette, C., Tremblay, B., & Newton, R. (2019). Winter coastal divergence as a predictor for the minimum sea ice extent in the Laptev Sea. *Journal of Climate*, *32*(4), 1063–1080. doi: https://doi.org/10.1175/JCLI-D-18-0169.1

Budikova, D. (2009). Role of Arctic sea ice in global atmospheric circulation: A review. *Global and Planetary Change*, *68*(3), 149–163. doi: https://doi.org/10.1016/j.gloplacha.2009.04.001

Comiso, J. C. (2012). Large decadal decline of the Arctic multiyear ice cover. *Journal of Climate*, *25*, 1176–1193. doi: https://doi.org/10.1175/JCLI-D-11-00113.1

Comiso, J. C., Meier, W. N., & Gersten, R. (2017). Variability and trends in the Arctic sea ice cover: Results from different techniques. *Journal of Geophysical Research: Oceans*, *122*(8), 6883–6900. doi: https://doi.org/10.1002/2017JC012768

Comiso, J. C., Parkinson, C. L., Gersten, R., & Stock, L. (2008). Accelerated decline in the Arctic sea ice cover. *Geophysical Research Letters*, *35*(1). doi: https://doi.org/10.1029/2007GL031972

DeRepentigny, P., Tremblay, L. B., Newton, R., & Pfirman, S. (2016). Patterns of Sea Ice Retreat in the Transition to a Seasonally Ice-Free Arctic. *Journal of Climate*, *29*(19), 6993–7008. doi: https://doi.org/10.1175/JCLI-D-15-0733.1

Eicken, H. (2004). The role of Arctic sea ice in transporting and cycling terrigenous organic matter. In *The organic carbon cycle in the arctic ocean* (pp. 45–53). Springer Berlin.

Eicken, H., Kolatschek, J., Freitag, J., Lindemann, F., Kassens, H., & Dmitrenko, I. (2000).

A key source area and constraints on entrainment for basin-scale sediment transport by Arctic sea ice. *Geophysical Research Letters*, *27*(13), 1919–1922. doi: https://doi.org/10.1029/1999GL011132

Emmerson, C., & Lahn, G. (2012). *Arctic Opening: Opportunity and Risk in the High North* (Tech. Rep.). London, United Kingdom: Chatham House. (Available at: `https://www.chathamhouse.org/publications/papers/view/182839`)

England, M., Jahn, A., & Polvani, L. (2019). Nonuniform Contribution of Internal Variability to Recent Arctic Sea Ice Loss. *Journal of Climate*, *32*(13), 4039–4053. doi: https://doi.org/10.1175/JCLI-D-18-0864.1

Fernández-Méndez, M., Katlein, C., Rabe, B., Nicolaus, M., Peeken, I., Bakker, K., … Boetius, A. (2015). Photosynthetic production in the central Arctic Ocean during the record sea-ice minimum in 2012. *Biogeosciences*, *12*(11), 3525–3549. doi: https://doi.org/10.5194/bg-12-3525-2015

Fingas, M., & Hollebone, B. (2003). Review of behaviour of oil in freezing environments. *Marine Pollution Bulletin*, *47*(9-12), 333–340. doi: https://doi.org/10.1016/S0025-326X(03)00210-8

Flanders Marine Institute. (2018). *Maritime Boundaries Geodatabase: Maritime Boundaries and Exclusive Economic Zones (200NM), version 10.* doi: https://doi.org/10.14284/312

Fowler, C., Emery, W., & Maslanik, J. (2004). Satellite-derived evolution of Arctic sea ice age: October 1978 to March 2003. *Geoscience and Remote Sensing Letters, IEEE*, *1*(2), 71–74. doi: https://doi.org/10.1109/LGRS.2004.824741

Glickson, D., Grabowski, M., Coolbaugh, T., Dickins, D., Glenn, R., Lee, K., … others (2014). Responding to oil spills in the U.S. Arctic marine environment. In *International oil spill conference proceedings* (Vol. 2014, p. 283740). doi: https://doi.org/10.7901/2169-3358-2014-1-283740.1

Gradinger, R. R., Kaufman, M. R., & Bluhm, B. A. (2009). Pivotal role of sea ice sediments in the seasonal development of near-shore Arctic fast ice biota. *Marine Ecology Progress Series*, *394*, 49–63. doi: https://doi.org/10.3354/meps08320

Hurrell, J. W., Holland, M. M., Gent, P. R., Ghan, S., Kay, J. E., Kushner, P. J., … others (2013). The Community Earth System Model: a framework for collaborative research. *Bulletin of the American Meteorological Society*, *94*(9), 1339–1360. doi: https://doi.org/10.1175/BAMS-D-12-00121.1

Izumiyama, K., Uto, S., Sakai, S., et al. (2004). Prediction of oil-ice sandwich formation. *International Journal of Offshore and Polar Engineering*, *14*(03).

Jahn, A. (2018). Reduced probability of ice-free summers for 1.5°C compared to 2°C warming. *Nature Climate Change*, *8*(5), 409. doi: https://doi.org/10.1038/s41558-018-0127-8

Jahn, A., & Holland, M. M. (2013). Implications of Arctic sea ice changes for North Atlantic deep convection and the meridional overturning circulation in CCSM4-CMIP5 simulations. *Geophysical Research Letters*, *40*(6), 1206–1211. doi: https://doi.org/10.1002/grl.50183

Jahn, A., Kay, J. E., Holland, M. M., & Hall, D. M. (2016). How predictable is the timing of a summer ice-free Arctic? *Geophysical Research Letters*, *43*(17), 9113–9120. doi: https://doi.org/10.1002/2016GL070067

Jin, M., Deal, C., Wang, J., Alexander, V., Gradinger, R., Saitoh, S.-I., … Stabeno, P. (2007). Ice-associated phytoplankton blooms in the southeastern Bering Sea. *Geophysical Research Letters*, *34*(6). doi: https://doi.org/10.1029/2006GL028849

Jones, C., Robertson, E., Arora, V., Friedlingstein, P., Shevliakova, E., Bopp, L., … others (2013). Twenty-first-century compatible CO2 emissions and airborne fraction simulated by CMIP5 earth system models under four representative concentration pathways. *Journal of Climate*, *26*(13), 4398–4413. doi: https://doi.org/10.1175/JCLI-D-12-00554.1

Kay, J. E., Deser, C., Phillips, A., Mai, A., Hannay, C., Strand, G., … Vertenstein, M. (2015). The Community Earth System Model (CESM) Large Ensemble Project: A Community Resource for Studying Climate Change in the Presence of Internal Climate Variability. *Bulletin of the American Meteorological Society*, *96*(8), 1333-1349. doi: https://doi.org/10.1175/BAMS-D-13-00255.1

Krumpen, T., Belter, H. J., Boetius, A., Damm, E., Haas, C., Hendricks, S., … Stein, R. (2019). Arctic warming interrupts the Transpolar Drift and affects long-range transport of sea ice and ice-rafted matter. *Scientific Reports*, *9*(5459), 1–9. doi: https://doi.org/10.1038/s41598-019-41456-y

Kwok, R. (2018). Arctic sea ice thickness, volume, and multiyear ice coverage: losses and coupled variability (1958–2018). *Environmental Research Letters*, *13*(10), 105005. doi: https://doi.org/10.1088/1748-9326/aae3ec

Labe, Z., Magnusdottir, G., & Stern, H. (2018). Variability of Arctic sea ice thickness using

PIOMAS and the CESM Large Ensemble. *Journal of Climate*, *31*(8), 3233–3247. doi: https://doi.org/10.1175/JCLI-D-17-0436.1

Maslanik, J., Fowler, C., Stroeve, J., Drobot, S., Zwally, J., Yi, D., & Emery, W. (2007). A younger, thinner Arctic ice cover: Increased potential for rapid, extensive sea-ice loss. *Geophysical Research Letters*, *34*(24). doi: https://doi.org/10.1029/2007GL032043

Massonnet, F., Fichefet, T., Goosse, H., Bitz, C. M., Philippon-Berthier, G., Holland, M. M., & Barriat, P.-Y. (2012). Constraining projections of summer Arctic sea ice. *The Cryosphere*, *6*(6), 1383–1394. doi: https://doi.org/10.5194/tc-6-1383-2012

Meier, W., Fetterer, F., Savoie, M., Mallory, S., Duerr, R., & Stroeve, J. (2017). NOAA/NSIDC Climate Data Record of Passive Microwave Sea Ice Concentration, Version 3 Revision 1 [monthly averages from January 1989 to December 2008]. *National Snow and Ice Data Center, Boulder, Colorado, USA*, Accessed July 2018. doi: https://doi.org/10.7265/N59P2ZTG

Melnikov, I. A., Kolosova, E. G., Welch, H. E., & Zhitina, L. S. (2002). Sea ice biological communities and nutrient dynamics in the Canada Basin of the Arctic Ocean. *Deep Sea Research Part I: Oceanographic Research Papers*, *49*(9), 1623–1649. doi: https://doi.org/10.1016/S0967-0637(02)00042-0

Newton, R., Pfirman, S., Schlosser, P., Tremblay, B., Murray, M., & Pomerance, R. (2016). White Arctic vs. Blue Arctic: A case study of diverging stakeholder responses to environmental change. *Earth's Future*, *4*(8), 396–405. doi: https://doi.org/10.1002/2016EF000356

Newton, R., Pfirman, S., Tremblay, B., & DeRepentigny, P. (2017). Increasing transnational sea-ice exchange in a changing Arctic Ocean. *Earth's Future*, *5*(6), 633–647. doi: https://doi.org/10.1002/2016EF000500

Newton, R., Schlosser, P., Mortlock, R., Swift, J., & MacDonald, R. (2013). Canadian Basin freshwater sources and changes: Results from the 2005 Arctic Ocean Section. *Journal of Geophysical Research: Oceans*, *118*(4), 2133–2154. doi: https://doi.org/10.1002/jgrc.20101

Ng, A. K., Andrews, J., Babb, D., Lin, Y., & Becker, A. (2018). Implications of climate change for shipping: Opening the Arctic seas. *Wiley Interdisciplinary Reviews: Climate Change*, *9*(2), e507. doi: https://doi.org/10.1002/wcc.507

Niederdrenk, A. L., & Notz, D. (2018). Arctic sea ice in a 1.5 C warmer world. *Geophysical Research Letters*, *45*(4), 1963–1971. doi: https://doi.org/10.1002/2017GL076159

Nordquist, M. (2011). *United Nations Convention on the Law of the Sea 1982, Volume VII: A Commentary.* Brill. doi: https://doi.org/10.1163/ej.9789004191174.iii-488

Nürnberg, D., Wollenburg, I., Dethleff, D., Eicken, H., Kassens, H., Letzig, T., … Thiede, J. (1994). Sediments in Arctic sea ice: Implications for entrainment, transport and release. *Marine Geology*, *119*(3-4), 185–214. doi: https://doi.org/10.1016/0025-3227(94)90181-3

Obbard, R. W., Sadri, S., Wong, Y. Q., Khitun, A. A., Baker, I., & Thompson, R. C. (2014). Global warming releases microplastic legacy frozen in Arctic Sea ice. *Earth's Future*, *2*(6), 315–320. doi: https://doi.org/10.1002/2014EF000240

Octaviani, M., Stemmler, I., Lammel, G., & Graf, H. F. (2015). Atmospheric transport of persistent organic pollutants to and from the Arctic under present-day and future climate. *Environmental science & technology*, *49*(6), 3593–3602. doi: https://doi.org/10.1021/es505636g

Ogi, M., & Rigor, I. G. (2013). Trends in Arctic sea ice and the role of atmospheric circulation. *Atmospheric Science Letters*, *14*(2), 97–101. doi: https://doi.org/10.1002/asl2.423

Olsen, L. M., Laney, S. R., Duarte, P., Kauko, H. M., Fernández-Méndez, M., Mundy, C. J., … others (2017). The seeding of ice algal blooms in Arctic pack ice: the multiyear ice seed repository hypothesis. *Journal of Geophysical Research: Biogeosciences*, *122*(7), 1529–1548. doi: https://doi.org/10.1002/2016JG003668

Ostreng, W., Eger, K. M., Fløistad, B., Jørgensen-Dahl, A., Lothe, L., Mejlænder-Larsen, M., & Wergeland, T. (2013). *Shipping in arctic waters: a comparison of the northeast, northwest and trans polar passages.* Springer Science & Business Media. doi: 10.1007/978-3-642-16790-4

Peeken, I., Primpke, S., Beyer, B., Gütermann, J., Katlein, C., Krumpen, T., … Gerdts, G. (2018). Arctic sea ice is an important temporal sink and means of transport for microplastic. *Nature communications*, *9*(1), 1505. doi: https://doi.org/10.1038/s41467-018-03825-5

Peng, G., Meier, W., Scott, D., & Savoie, M. (2013). A long-term and reproducible passive microwave sea ice concentration data record for climate studies and monitoring. *Earth System Science Data*, *5*(2), 311–318. doi: https://doi.org/10.5194/essd-5-311-2013

Peterson, C. H., Rice, S. D., Short, J. W., Esler, D., Bodkin, J. L., Ballachey, B. E., & Irons, D. B. (2003). Long-term ecosystem response to the Exxon Valdez oil spill. *Science*, *302*(5653), 2082–2086. doi: 10.1126/science.1084282

Pfirman, S., Eicken, H., Bauch, D., & Weeks, W. (1995). The potential transport of pollutants by Arctic sea ice. *Science of the Total Environment*, *159*(2-3), 129–146. doi: https://doi.org/10.1016/0048-9697(95)04174-Y

Pfirman, S., Haxby, W. F., Colony, R., & Rigor, I. (2004). Variability in Arctic sea ice drift. *Geophysical Research Letters*, *31*(16). doi: https://doi.org/10.1029/2004GL020063

Pfirman, S., Kögeler, J., & Rigor, I. (1997). Potential for rapid transport of contaminants from the Kara Sea. *Science of the Total Environment*, *202*(1-3), 111–122. doi: https://doi.org/10.1016/S0048-9697(97)00108-3

Post, E., Forchhammer, M. C., Bret-Harte, M. S., Callaghan, T. V., Christensen, T. R., Elberling, B., … others (2009). Ecological dynamics across the Arctic associated with recent climate change. *Science*, *325*(5946), 1355–1358. doi: https://doi.org/10.1126/science.1173113

Rigor, I. G., & Wallace, J. M. (2004). Variations in the age of Arctic sea-ice and summer sea-ice extent. *Geophysical Research Letters*, *31*(9). doi: https://doi.org/10.1029/2004GL019492

Sanderson, B. M., Xu, Y., Tebaldi, C., Wehner, M., O'Neill, B. C., Jahn, A., … others (2017). Community climate simulations to assess avoided impacts in 1.5 and 2°C futures. *Earth System Dynamics*, *8*(3), 827–847. doi: https://doi.org/10.5194/esd-8-827-2017

Schøyen, H., & Bråthen, S. (2011). The Northern Sea Route versus the Suez Canal: cases from bulk shipping. *Journal of Transport Geography*, *19*(4), 977–983. doi: https://doi.org/10.1016/j.jtrangeo.2011.03.003

Screen, J. A., & Williamson, D. (2017). Ice-free Arctic at 1.5° C? *Nature Climate Change*, *7*(4), 230. doi: https://doi.org/10.1038/nclimate3248

Shevchenko, V. P., Vinogradova, A. A., Lisitzin, A. P., Novigatsky, A. N., Panchenko, M. V., & Pol'kin, V. V. (2016). Aeolian and Ice Transport of Matter (Including Pollutants) in the Arctic. In R. Kallenborn (Ed.), *Implications and consequences of anthropogenic pollution in polar environments* (pp. 59–73). Berlin, Heidelberg: Springer Berlin Heidelberg. doi: https://doi.org/10.1007/978-3-642-12315-3_5

Sigmond, M., Fyfe, J. C., & Swart, N. C. (2018). Ice-free Arctic projections under the Paris Agreement. *Nature Climate Change*, *8*(5), 404. doi: https://doi.org/10.1038/s41558-018-0124-y

SIMIP Community. (2020). Arctic Sea Ice in CMIP6. *Geophysical Research Letters*. (under review)

Smedsrud, L. H. (2001). Frazil-ice entrainment of sediment: large-tank laboratory experiments. *Journal of Glaciology*, *47*(158), 461–471. doi: https://doi.org/10.3189/172756501781832142

Smedsrud, L. H. (2002). A model for entrainment of sediment into sea ice by aggregation between frazil-ice crystals and sediment grains. *Journal of Glaciology*, *48*(160), 51–61. doi: https://doi.org/10.3189/172756502781831520

Smith, A., & Jahn, A. (2019). Definition differences and internal variability affect the simulated Arctic sea ice melt season. *The Cryosphere*, *13*(1), 1–20. doi: https://doi.org/10.5194/tc-13-1-2019

Sørstrøm, S. E., Brandvik, P. J., Buist, I., Daling, P., Dickins, D., Faksness, L.-G., … Singsaas, I. (2010). *Joint industry program on oil spill contingency for Arctic and ice-covered waters: Summary report*. Trondheim, Norway: SINTEF.

Stephenson, S. R., Smith, L. C., Brigham, L. W., & Agnew, J. A. (2013). Projected 21st-century changes to Arctic marine access. *Climatic Change*, *118*(3-4), 885–899. doi: https://doi.org/10.1007/s10584-012-0685-0

Stroeve, J., Barrett, A., Serreze, M., & Schweiger, A. (2014). Using records from submarine, aircraft and satellites to evaluate climate model simulations of Arctic sea ice thickness. *Cryosphere*, *8*(5). doi: https://doi.org/10.5194/tc-8-1839-2014

Stroeve, J., Kattsov, V., Barrett, A., Serreze, M., Pavlova, T., Holland, M., & Meier, W. N. (2012). Trends in Arctic sea ice extent from CMIP5, CMIP3 and observations. *Geophysical Research Letters*, *39*(16). doi: https://doi.org/10.1029/2012GL052676

Stroeve, J., Markus, T., Boisvert, L., Miller, J., & Barrett, A. (2014). Changes in Arctic melt season and implications for sea ice loss. *Geophysical Research Letters*, *41*(4), 1216–1225. doi: https://doi.org/10.1002/2013GL058951

Stroeve, J., & Notz, D. (2018). Changing state of Arctic sea ice across all seasons. *Environmental Research Letters*, *13*(10), 103001. doi: https://doi.org/10.1088/1748-9326/aade56

Stroeve, J., Serreze, M., Holland, M. M., Kay, J. E., Malanik, J., & Barrett, A. P. (2012). The Arctic's rapidly shrinking sea ice cover: a research synthesis. *Climatic Change*, *110*(3-4), 1005–1027. doi: https://doi.org/10.1007/s10584-011-0101-1

Swart, N. C., Fyfe, J. C., Hawkins, E., Kay, J. E., & Jahn, A. (2015). Influence of internal variability on Arctic sea-ice trends. *Nature Climate Change*, *5*(2), 86. doi: https://

doi.org/10.1038/nclimate2483

Tandon, N. F., Kushner, P. J., Docquier, D., Wettstein, J. J., & Li, C. (2018). Reassessing Sea Ice Drift and Its Relationship to Long-Term Arctic Sea Ice Loss in Coupled Climate Models. *Journal of Geophysical Research: Oceans*, *123*(6), 4338–4359. doi: https://doi.org/10.1029/2017JC013697

Tremblay, L., Schmidt, G., Pfirman, S., Newton, R., & Derepentigny, P. (2015). Is ice-rafted sediment in a North Pole marine record evidence for perennial sea-ice cover? *Philosophical Transactions of the Royal Society A: Mathematical, Physical and Engineering Sciences*, *373*(2052), 20140168. doi: https://doi.org/10.1098/rsta.2014.0168

Tschudi, M., Fowler, C., Maslanik, J., Stewart, J. S., & Meier, W. (2016). Polar Pathfinder Daily 25 km EASE-Grid Sea Ice Motion Vectors, Version 3 [monthly averages from January 1989 to December 2008]. *NASA National Snow and Ice Data Center Distributed Active Archive Center, Boulder, Colorado, USA*, Accessed March 2016. doi: http://dx.doi.org/10.5067/O57VAIT2AYYY

UNFCCC. (2015). *Adoption of the Paris Agreement, FCCC/CP/2015/10/Add.1.* (Available at: `https://unfccc.int/resource/docs/2015/cop21/eng/10a01.pdf`)

Varotsos, C. A., & Krapivin, V. F. (2018). Pollution of Arctic Waters Has Reached a Critical Point: an Innovative Approach to This Problem. *Water, Air, & Soil Pollution*, *229*(11), 343. doi: https://doi.org/10.1007/s11270-018-4004-x

Venkatesh, S., El-Tahan, H., Comfort, G., & Abdelnour, R. (1990). Modelling the behaviour of oil spills in ice-infested waters. *Atmosphere-Ocean*, *28*(3), 303–329. doi: https://doi.org/10.1080/07055900.1990.9649380

Wang, M., & Overland, J. E. (2009). A sea ice free summer Arctic within 30 years? *Geophysical Research Letters*, *36*(7). doi: https://doi.org/10.1029/2009GL037820

Wang, M., & Overland, J. E. (2012). A sea ice free summer Arctic within 30 years: An update from CMIP5 models. *Geophysical Research Letters*, *39*(18). doi: https://doi.org/10.1029/2012GL052868

Wilhelmsen, J. M., & Gjerde, K. L. (2018). Norway and Russia in the Arctic: New Cold War Contamination? *Arctic Review on Law and Politics*, *9*, 381–407. doi: https://doi.org/10.23865/arctic.v9.1334

Wilkinson, J., Beegle-Krause, C. J., Evers, K.-U., Hughes, N., Lewis, A., Reed, M., & Wadhams, P. (2017). Oil spill response capabilities and technologies for ice-covered Arctic marine waters: A review of recent developments and established practices.

Ambio, *46*(3), 423–441. doi: https://doi.org/10.1007/s13280-017-0958-y

Williams, J., Tremblay, B., Newton, R., & Allard, R. (2016). Dynamic preconditioning of the minimum September sea-ice extent. *Journal of Climate*, *29*(16), 5879–5891. doi: https://doi.org/10.1175/JCLI-D-15-0515.1

Zappa, G., Pithan, F., & Shepherd, T. G. (2018). Multimodel evidence for an atmospheric circulation response to Arctic sea ice loss in the CMIP5 future projections. *Geophysical research letters*, *45*(2), 1011–1019. doi: https://doi.org/10.1002/2017GL076096

Supporting Information for "Increased Transnational Sea Ice Transport Between Neighboring Arctic States in the 21st Century"

Patricia DeRepentigny[1,2], Alexandra Jahn[1], L. Bruno Tremblay[2,3], Robert Newton[3], and Stephanie Pfirman[4]

[1]Department of Atmospheric and Oceanic Sciences and Institute of Arctic and Alpine Research, University of Colorado Boulder, Boulder, Colorado, USA.

[2]Department of Atmospheric and Oceanic Sciences, McGill University, Montreal, Quebec, Canada.

[3]Lamont-Doherty Earth Observatory, Columbia University, Palisades, New York, USA.

[4]School of Sustainability, Arizona State University, Tempe, Arizona, USA.

Corresponding author: P. DeRepentigny, Department of Atmospheric and Oceanic Sciences, University of Colorado Boulder, 311 UCB, Boulder, CO 80309, USA. (patricia.derepentigny@colorado.edu)

Contents of this file

Text S1. Observational Datasets

The National Snow and Ice Data Center's (NSIDC) Polar Pathfinder project provides sea ice motion vectors on the 25 km EASE-Grid from the beginning of polar-orbiting satellite observations in November 1978 to 2017 (Tschudi et al., 2016). This gridded product is derived through optimal interpolation of observations from the International Arctic Buoy Program (IABP), as well as the Scanning Multichannel Microwave Radiometer (SMMR), the Special Sensor Microwave Imager (SSM/I), the Special Sensor Microwave Imager Sounder (SSMIS), the Advanced Microwave Scanning Radiometer - Earth Observing System (AMSR-E) and the Advanced Very High Resolution Radiometer (AVHRR) sensors. It is complemented with free drift estimates derived from 10 m winds provided by the National Centers for Environmental Prediction and the National Center for Atmospheric Research (NCEP/NCAR) reanalysis dataset where no observations were available. We also use sea ice concentration data derived from passive microwave brightness temperature from the National Oceanic and Atmospheric Administration (NOAA)/NSIDC Climate Data Record (Meier et al., 2017; Peng et al., 2013). It is a product of different algorithms used to combine observations made by the SMMR, SSM/I and SSMIS sensors, available from late 1978 to 2017.

The Polar Pathfinder and Climate Data Record datasets were previously used in Newton, Pfirman, Tremblay, and DeRepentigny (2017), where a similar analysis of transnational ice exchange over the observational period was performed. Newton et al. (2017) used a weekly time resolution while we here use a monthly resolution to allow for a direct comparison with model data, which is only available at a monthly resolution for one of the two forcing scenarios analyzed here (see section 2.1). The reduction of temporal resolution from weekly to monthly has been shown to lead to an increase of the error in drift distance when compared to buoy data by approximately 45 km (less than two grid cells) after a year of tracking when using the ice tracking system (DeRepentigny et al., 2016). In the context of this study, we find that the flux of transnational ice is reduced slightly towards the end of the 21st century for most pathways when going from a monthly to a weekly resolution (Figure S2). However, none of the conclusions from this study are affected by the change in time resolution from monthly to weekly.

All observational analyses presented here use satellite-derived sea ice velocity and concentration between January 1989 and December 2008. We begin the analysis in 1989 to avoid earlier satellite-based drift vectors, based on retrievals from the relatively low-resolution SMMR sensor, that exhibit a low bias in sea ice velocity compared to co-located buoy data (Bruno Tremblay, Robert Newton and Charles Brunette, personal communication, May 16, 2019). Comparison between observations and model data presented in section S2 is therefore done over the 20-year period of 1989–2008.

Text S2. Comparison of the CESM with Observations

To provide an assessment of the performance of the CESM in simulating sea ice transport between the different EEZs of the Arctic, we compare CESM results to results from SITU using satellite observations from the period of 1989 to 2008. We find that the annual cycle of areal ice formation and melt in the CESM-LE compares well with the observations (Figure S3). Ice formation peaks in October and ice melt peaks in August (peak of ice formation/melt here refers to the month with the largest area of simulated ice formation/melt using SITU). Note, however, that the average amount of formation and melt area obtained from the observations does not fall within the spread of internal variability of the CESM-LE during the months of peak ice formation and melt (i.e., October and August, respectively), with the CESM-LE simulating too little ice formation and melt (Figure S3). The spatial distributions of areal ice formation and melt are also well represented in the CESM-LE (Figures S4 and S5) despite slightly larger frequencies of detected fall formation and summer melt over the peripheral seas for the observations (in agreement with results presented in Figure S3).

The exchange of transnational ice between the different EEZs of the Arctic simulated by the CESM-LE over the period of 1989–2008 is in good general agreement with observations (Figure S6). Both the observations and the CESM-LE show that most of the transnational ice formed in Canada melts in the US EEZ, most of the transnational ice formed in the United States melts in Russia, and most of the Russian transnational ice melts in Norway (Figure S6; see also Newton et al., 2017). However, the observed transnational ice transport is slightly outside the range of internal variability of the CESM-LE for two pathways: (1) ice forming in the United States and melting in Russia is underestimated in the CESM, and (2) ice forming in Russia and melting in Norway and Iceland is overestimated in the CESM (Figure S6).

The small inconsistencies in areal flux of US ice towards Russia and Russian ice towards Norway and Iceland between observations and the CESM-LE do not extend throughout the full area of the EEZ of formation, but are present only in the region directly upstream of the EEZ of melt, following the general Arctic sea ice circulation (Figure S7). For the slightly lower simulated flux of US ice towards Russia by the CESM compared to observations (Figure S6), there is a smaller area of high transnational ice promotion probability within the US EEZ close to the Russian border for the CESM-LE compared to the observations (Figures S7a, S7b, and S7d). The slightly higher flux of Russian ice towards Norway and Iceland in the CESM-LE (Figure S6) is mainly driven by higher simulated probabilities of transnational ice promotion in the Kara and Barents Seas than what is observed (Figures S7a–S7c).

Differences in transnational ice exchange between the CESM-LE and observations for US ice melting in Russia and Russian ice melting in Norway and Iceland can be attributed to a bias in the simulated atmospheric circulation over the Arctic during the ice-covered season and the resulting sea ice circulation anomalies. DeRepentigny et al. (2016) showed that the variability in winter sea-level pressure in the CESM-LE results in higher sea ice velocities off the coast of Russia in the Kara and Barents Seas compared to observations, transporting more ice away from the coast and into the Transpolar Drift Stream (see their Figures 6c and 6d). Moreover, the observations are characterized by a strong current along the coast of Alaska, which is not simulated in the years of low winter sea-level pressure in the CESM-LE (see their Figures 6a and 6b). As one would expect, sea ice motion, and consequently transnational ice exchange, is intimately linked to the atmospheric circulation over the Arctic that drives the sea ice.

References

DeRepentigny, P., Tremblay, L. B., Newton, R., & Pfirman, S. (2016). Patterns of Sea Ice Retreat in the Transition to a Seasonally Ice-Free Arctic. *Journal of Climate*, *29*(19), 6993–7008. doi: https://doi.org/10.1175/JCLI-D-15-0733.1

Meier, W., Fetterer, F., Savoie, M., Mallory, S., Duerr, R., & Stroeve, J. (2017). NOAA/NSIDC Climate Data Record of Passive Microwave Sea Ice Concentration, Version 3 Revision 1 [monthly averages from January 1989 to December 2008]. *National Snow and Ice Data Center, Boulder, Colorado, USA*, Accessed July 2018. doi: https://doi.org/10.7265/N59P2ZTG

Newton, R., Pfirman, S., Tremblay, B., & DeRepentigny, P. (2017). Increasing transnational sea-ice exchange in a changing Arctic Ocean. *Earth's Future*, *5*(6), 633–647. doi: https://doi.org/10.1002/2016EF000500

Peng, G., Meier, W., Scott, D., & Savoie, M. (2013). A long-term and reproducible passive microwave sea ice concentration data record for climate studies and monitoring. *Earth System Science Data*, *5*(2), 311–318. doi: https://doi.org/10.5194/essd-5-311-2013

Tschudi, M., Fowler, C., Maslanik, J., Stewart, J. S., & Meier, W. (2016). Polar Pathfinder Daily 25 km EASE-Grid Sea Ice Motion Vectors, Version 3 [monthly averages from January 1989 to December 2008]. *NASA National Snow and Ice Data Center Distributed Active Archive Center, Boulder, Colorado, USA*, Accessed March 2016. doi: http://dx.doi.org/10.5067/O57VAIT2AYYY

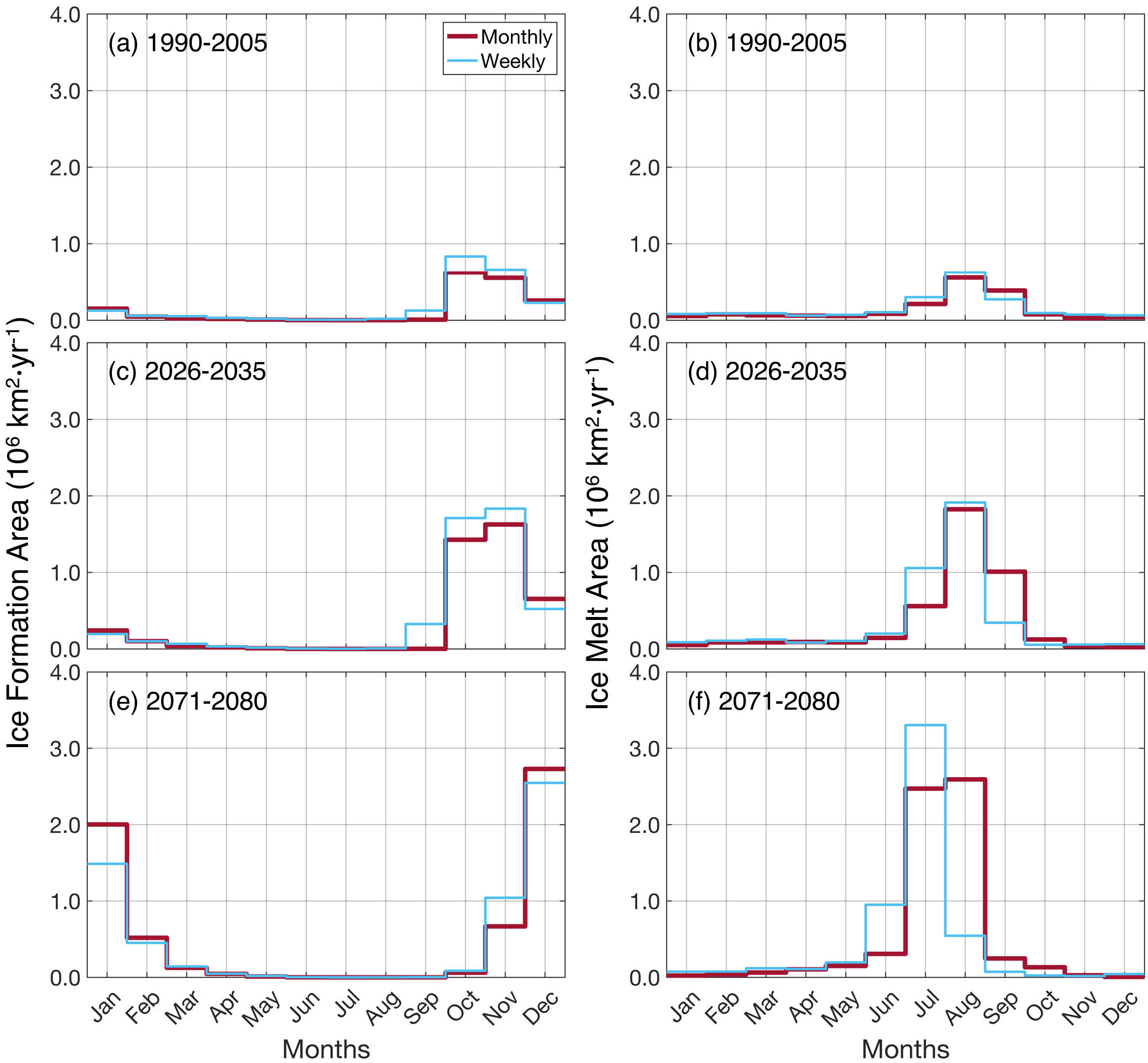

Figure S1: Annual cycle of ice formation (a, c, e) and melt (b, d, f) over the periods of 1990–2005 (a, b), 2026–2035 (c, d) and 2071–2080 (e, f) for the first 35 members of the CESM-LE using a monthly (burgundy) and weekly (light blue) time resolutions. Only ice floes that formed and melted between the specified time periods are considered. Note that some of the differences between the weekly and monthly time resolution can be attributed to the way weeks are distributed into months as every month contains either 29, 30 or 31 days and thus always includes part of a week.

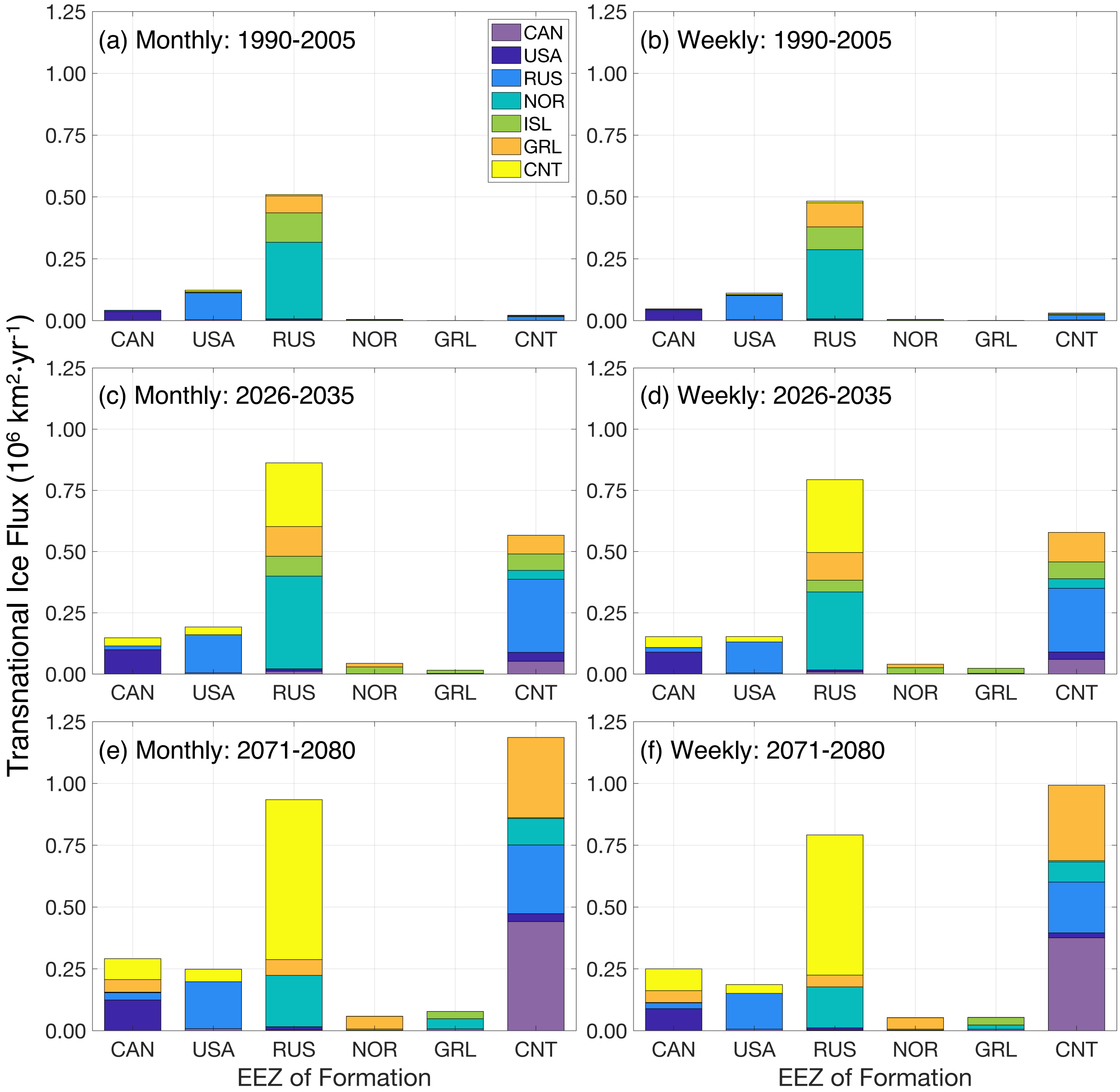

Figure S2: Annual mean average areal flux of transnational ice for the CESM-LE over the periods of 1990–2005 (a, b), 2026–2035 (c, d) and 2071–2080 (e, f) using a monthly (a, c, e) and weekly (b, d, f) time resolutions. The height of each colored portion within one bar represents the annual mean areal flux of ice between the EEZ of formation (x axis) and the EEZ of melt (color). Note that domestic ice is not included in this figure in order to focus on the features of transnational ice exchange.

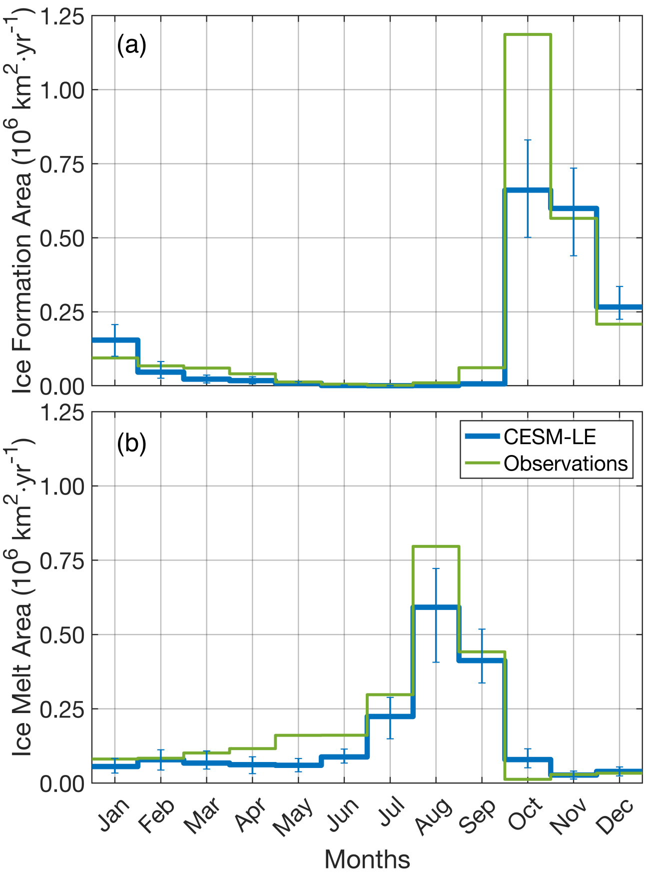

Figure S3: Annual cycle of mean areal ice formation (a) and melt (b) in the observations (green) and the CESM-LE (blue) for the period of 1989–2008. The error bars show the maximum and minimum 20-year averaged formation/melt area for each month across the 40 ensemble members of the CESM-LE, showing the range of internal variability for this ensemble. Only ice floes that formed and melted between 1989–2008 are considered. Note that the values shown here are not meant to represent the actual amount of ice that forms and melts in the Arctic every year, but rather the area of ice formation and melt we obtain from SITU (see section 2.2).

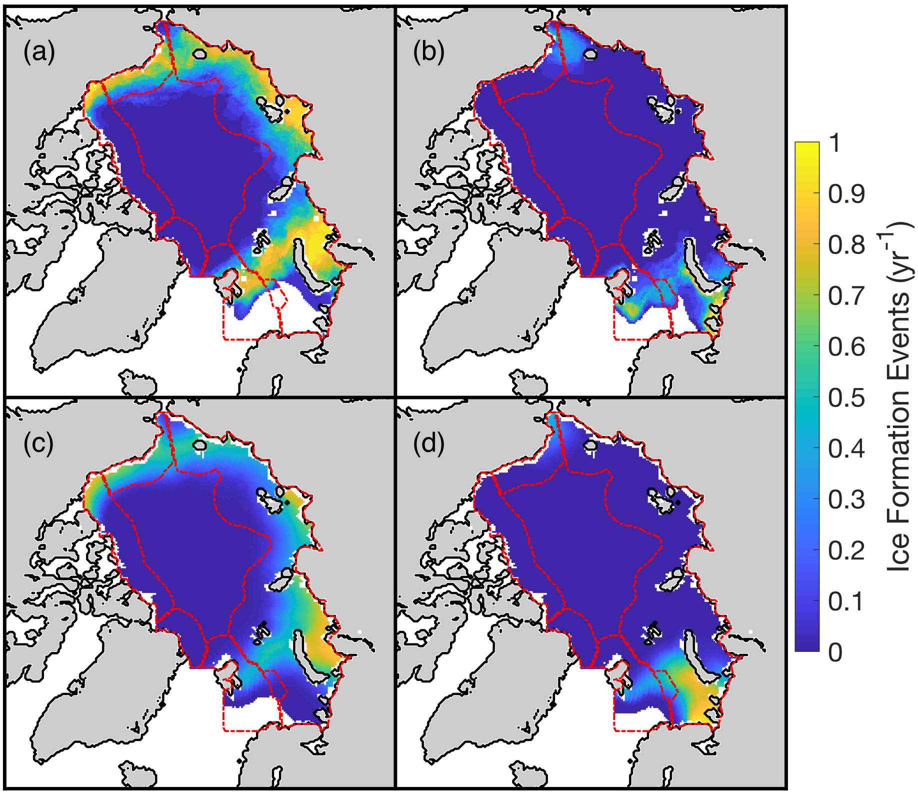

Figure S4: Average number of ice formation events per year in fall (SON) (a, c) and winter (DJF) (b, d) over the period of 1989–2008 for both observations (a, b) and the CESM-LE (c, d). The borders of the EEZs are indicated by red lines. Only ice floes that formed and melted between 1989–2008 are considered.

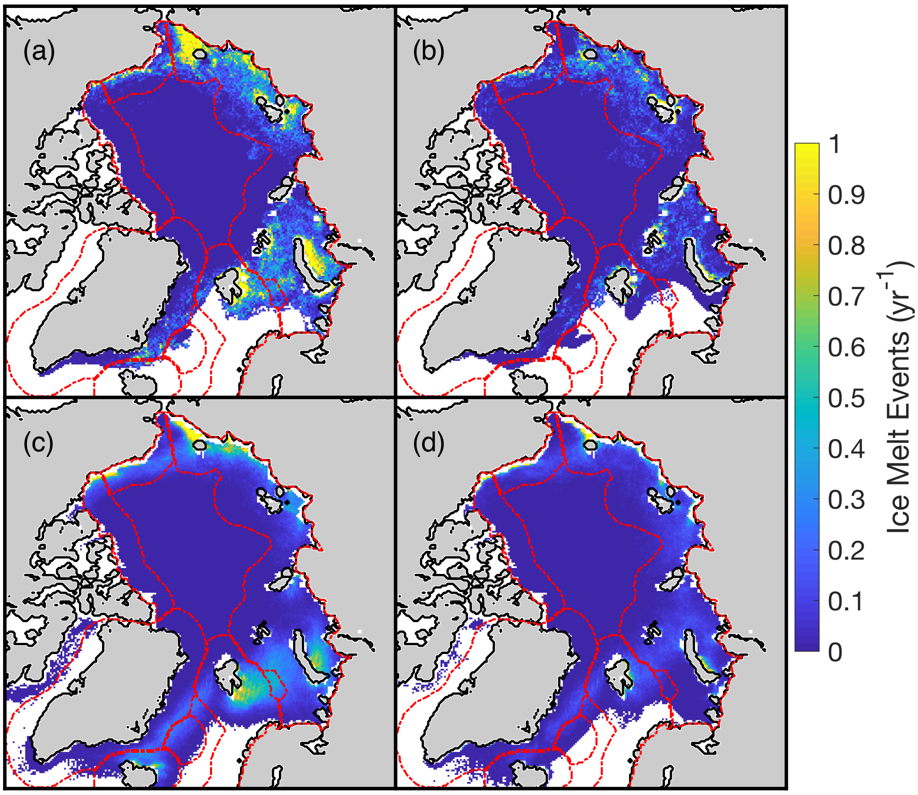

Figure S5: As in Figure S4, but for the average number of ice melt events per year in summer (JJA) (a, c) and fall (SON) (b, d).

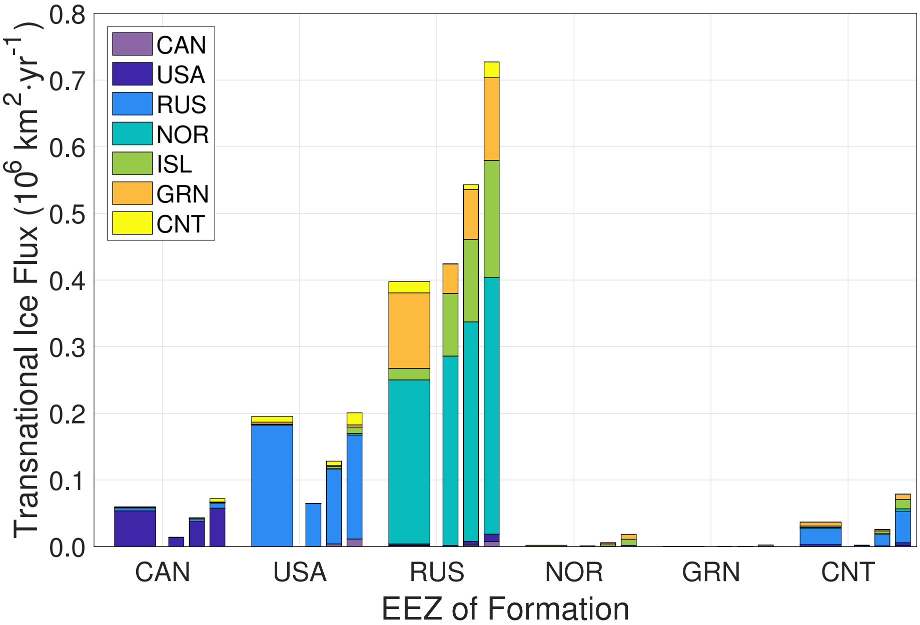

Figure S6: Annual mean areal transnational ice flux for the observations (wide bar) and annual mean minimum (left narrow bar), average (middle narrow bar) and maximum (right narrow bar) areal transnational ice flux for the 40 members of the CESM-LE for the period of 1989–2008. The height of each colored portion within one bar represents the annual mean areal flux of ice between the EEZ of formation (x axis) and the EEZ of melt (color). The CESM-LE is consistent with the observations when the observed value for each pathway lies between the range of the CESM-LE (minimum to maximum). Note that domestic ice is not included in this figure in order to focus on the features of transnational ice exchange.

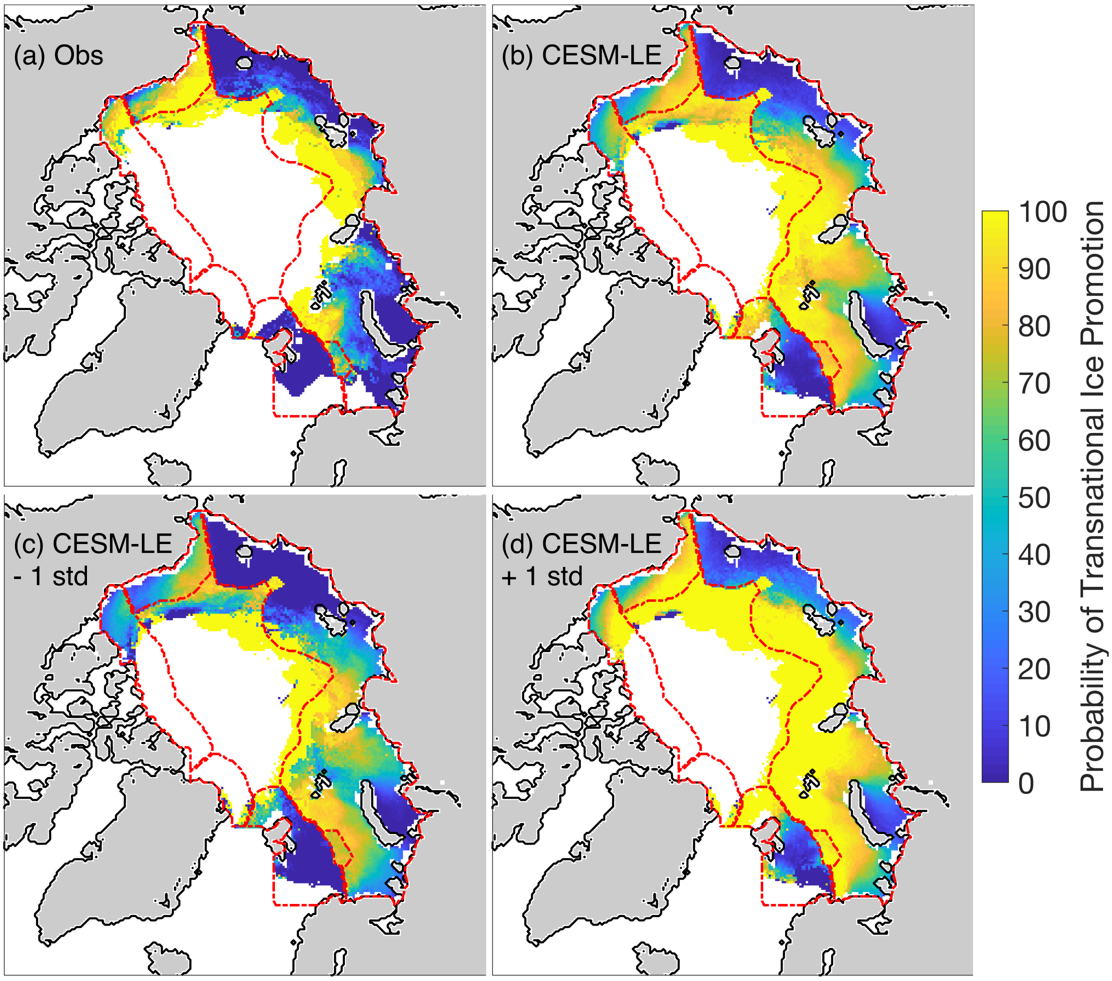

Figure S7: Probability of transnational ice promotion for observations (a), the ensemble mean of the CESM-LE (b) as well as the ensemble mean ± one standard deviation for the CESM-LE (c, d) over the period of 1989–2008. The color represents the probability that an ice parcel forming at each grid cell gets promoted from domestic ice to transnational ice. The borders of the EEZs are indicated by red lines. Note that the probability is calculated for each grid cell in which at least one ice parcel forms and thus gives no indication of how many ice parcels are considered in the calculation.

Table S1: Annual mean average areal flux of ice exchanged between all EEZs for the CESM-LE over the three time periods. The EEZ of formation is indicated in the first column and the EEZ of melt in the first row. All numbers are in km^2/year. The last column contains the total annual mean average areal flux of ice formed in each EEZ, only considering ice floes that melted before the end of the time period. The numbers in bold highlight the pathways that are statistically different between the CESM-LE and the CESM-LW over a same time period at the 95% confidence level using a t-test.

From/To	*Canada*	*USA*	*Russia*	*Norway*	*Iceland*	*Greenland*	*Central*	*Total*
				1981–2000				
Canada	39,426	32,741	3,177	32	218	96	631	76,321
USA	3,616	49,083	96,402	546	4,232	1,444	4,184	159,507
Russia	1,635	4,900	563,494	305,730	112,159	60,825	2,217	1,050,960
Norway	0	0	677	108,733	2,331	1,223	0	112,964
Greenland	0	0	0	4	113	31	0	148
Central	163	802	9,026	292	1,585	581	934	13,383
				2031–2050				
Canada	107,566	128,998	25,926	441	**1,563**	**4,855**	**62,049**	331,398
USA	6,297	105,809	176,848	0	**0**	0	**34,613**	323,567
Russia	**11,480**	10,188	1,597,911	**385,601**	**37,521**	**122,715**	**452,339**	2,617,755
Norway	10	0	737	135,196	33,191	**31,475**	18	200,627
Greenland	**789**	11	8	**10,823**	**41,205**	27,128	51	80,015
Central	**184,175**	52,953	352,701	**69,168**	81,513	**194,498**	833,752	1,768,760
				2081–2100				
Canada	327,395	**114,877**	33,716	**3,209**	**175**	**70,427**	**102,810**	652,609
USA	6,742	66,614	184,671	0	0	0	**60,638**	318,665
Russia	**2,495**	**13,346**	1,429,691	**162,929**	**4**	**40,631**	**654,681**	2,303,777
Norway	9	0	**1,692**	91,323	**1,331**	38,416	**821**	133,592
Greenland	**7,436**	**0**	64	**41,848**	**13,268**	177,128	603	240,347
Central	**437,773**	**17,441**	**250,289**	**111,080**	**410**	**310,993**	1,360,152	2,488,138

Table S2: As in Table S1, but for the CESM-LW and for the time periods of 2031–2050 and 2081–2100 only.

From/To	*Canada*	*USA*	*Russia*	*Norway*	*Iceland*	*Greenland*	*Central*	*Total*
2031–2050								
Canada	67,835	116,784	28,938	9	**401**	**423**	**38,568**	252,958
USA	4,134	102,824	181,077	3	**28**	20	**20,594**	308,680
Russia	**17,224**	13,310	1,529,744	**416,960**	**73,301**	**137,656**	**311,557**	2,499,752
Norway	0	0	918	137,622	29,449	**24,446**	0	192,435
Greenland	**97**	0	0	**4,560**	**25,810**	9,903	0	40,370
Central	**95,631**	53,653	357,849	**40,909**	78,207	**117,193**	540,412	1,283,854
2081–2100								
Canada	84,594	**139,616**	41,702	**85**	**1,153**	**2,207**	**67,080**	336,437
USA	3,884	95,500	196,153	0	0	0	**25,227**	320,764
Russia	**16,006**	**8,551**	1,600,756	**386,994**	**38,009**	**153,526**	**428,526**	2,632,368
Norway	51	0	**739**	130,358	**38,855**	35,565	**0**	205,568
Greenland	**1,307**	**125**	6	**8,969**	**51,634**	24,952	57	87,050
Central	**192,349**	**55,827**	**411,670**	**53,332**	**84,082**	**189,324**	813,423	1,800,007

Supporting Information for "Increased Transnational Sea Ice Transport Between Neighboring Arctic States in the 21st Century"

Patricia DeRepentigny[1,2], Alexandra Jahn[1], L. Bruno Tremblay[2,3], Robert Newton[3], and Stephanie Pfirman[4]

[1]Department of Atmospheric and Oceanic Sciences and Institute of Arctic and Alpine Research, University of Colorado Boulder, Boulder, Colorado, USA.

[2]Department of Atmospheric and Oceanic Sciences, McGill University, Montreal, Quebec, Canada.

[3]Lamont-Doherty Earth Observatory, Columbia University, Palisades, New York, USA.

[4]School of Sustainability, Arizona State University, Tempe, Arizona, USA.

Corresponding author: P. DeRepentigny, Department of Atmospheric and Oceanic Sciences, University of Colorado Boulder, 311 UCB, Boulder, CO 80309, USA. (patricia.derepentigny@colorado.edu)

Contents of this file

Text S1. Observational Datasets

The National Snow and Ice Data Center's (NSIDC) Polar Pathfinder project provides sea ice motion vectors on the 25 km EASE-Grid from the beginning of polar-orbiting satellite observations in November 1978 to 2017 (Tschudi et al., 2016). This gridded product is derived through optimal interpolation of observations from the International Arctic Buoy Program (IABP), as well as the Scanning Multichannel Microwave Radiometer (SMMR), the Special Sensor Microwave Imager (SSM/I), the Special Sensor Microwave Imager Sounder (SSMIS), the Advanced Microwave Scanning Radiometer - Earth Observing System (AMSR-E) and the Advanced Very High Resolution Radiometer (AVHRR) sensors. It is complemented with free drift estimates derived from 10 m winds provided by the National Centers for Environmental Prediction and the National Center for Atmospheric Research (NCEP/NCAR) reanalysis dataset where no observations were available. We also use sea ice concentration data derived from passive microwave brightness temperature from the National Oceanic and Atmospheric Administration (NOAA)/NSIDC Climate Data Record (Meier et al., 2017; Peng et al., 2013). It is a product of different algorithms used to combine observations made by the SMMR, SSM/I and SSMIS sensors, available from late 1978 to 2017.

The Polar Pathfinder and Climate Data Record datasets were previously used in Newton, Pfirman, Tremblay, and DeRepentigny (2017), where a similar analysis of transnational ice exchange over the observational period was performed. Newton et al. (2017) used a weekly time resolution while we here use a monthly resolution to allow for a direct comparison with model data, which is only available at a monthly resolution for one of the two forcing scenarios analyzed here (see section 2.1). The reduction of temporal resolution from weekly to monthly has been shown to lead to an increase of the error in drift distance when compared to buoy data by approximately 45 km (less than two grid cells) after a year of tracking when using the ice tracking system (DeRepentigny et al., 2016). In the context of this study, we find that the flux of transnational ice is reduced slightly towards the end of the 21st century for most pathways when going from a monthly to a weekly resolution (Figure S2). However, none of the conclusions from this study are affected by the change in time resolution from monthly to weekly.

All observational analyses presented here use satellite-derived sea ice velocity and concentration between January 1989 and December 2008. We begin the analysis in 1989 to avoid earlier satellite-based drift vectors, based on retrievals from the relatively low-resolution SMMR sensor, that exhibit a low bias in sea ice velocity compared to co-located buoy data (Bruno Tremblay, Robert Newton and Charles Brunette, personal communication, May 16, 2019). Comparison between observations and model data presented in section S2 is therefore done over the 20-year period of 1989–2008.

Text S2. Comparison of the CESM with Observations

To provide an assessment of the performance of the CESM in simulating sea ice transport between the different EEZs of the Arctic, we compare CESM results to results from SITU using satellite observations from the period of 1989 to 2008. We find that the annual cycle of areal ice formation and melt in the CESM-LE compares well with the observations (Figure S3). Ice formation peaks in October and ice melt peaks in August (peak of ice formation/melt here refers to the month with the largest area of simulated ice formation/melt using SITU). Note, however, that the average amount of formation and melt area obtained from the observations does not fall within the spread of internal variability of the CESM-LE during the months of peak ice formation and melt (i.e., October and August, respectively), with the CESM-LE simulating too little ice formation and melt (Figure S3). The spatial distributions of areal ice formation and melt are also well represented in the CESM-LE (Figures S4 and S5) despite slightly larger frequencies of detected fall formation and summer melt over the peripheral seas for the observations (in agreement with results presented in Figure S3).

The exchange of transnational ice between the different EEZs of the Arctic simulated by the CESM-LE over the period of 1989–2008 is in good general agreement with observations (Figure S6). Both the observations and the CESM-LE show that most of the transnational ice formed in Canada melts in the US EEZ, most of the transnational ice formed in the United States melts in Russia, and most of the Russian transnational ice melts in Norway (Figure S6; see also Newton et al., 2017). However, the observed transnational ice transport is slightly outside the range of internal variability of the CESM-LE for two pathways: (1) ice forming in the United States and melting in Russia is underestimated in the CESM, and (2) ice forming in Russia and melting in Norway and Iceland is overestimated in the CESM (Figure S6).

The small inconsistencies in areal flux of US ice towards Russia and Russian ice towards Norway and Iceland between observations and the CESM-LE do not extend throughout the full area of the EEZ of formation, but are present only in the region directly upstream of the EEZ of melt, following the general Arctic sea ice circulation (Figure S7). For the slightly lower simulated flux of US ice towards Russia by the CESM compared to observations (Figure S6), there is a smaller area of high transnational ice promotion probability within the US EEZ close to the Russian border for the CESM-LE compared to the observations (Figures S7a, S7b, and S7d). The slightly higher flux of Russian ice towards Norway and Iceland in the CESM-LE (Figure S6) is mainly driven by higher simulated probabilities of transnational ice promotion in the Kara and Barents Seas than what is observed (Figures S7a–S7c).

Differences in transnational ice exchange between the CESM-LE and observations for US ice melting in Russia and Russian ice melting in Norway and Iceland can be attributed to a bias in the simulated atmospheric circulation over the Arctic during the ice-covered season and the resulting sea ice circulation anomalies. DeRepentigny et al. (2016) showed that the variability in winter sea-level pressure in the CESM-LE results in higher sea ice velocities off the coast of Russia in the Kara and Barents Seas compared to observations, transporting more ice away from the coast and into the Transpolar Drift Stream (see their Figures 6c and 6d). Moreover, the observations are characterized by a strong current along the coast of Alaska, which is not simulated in the years of low winter sea-level pressure in the CESM-LE (see their Figures 6a and 6b). As one would expect, sea ice motion, and consequently transnational ice exchange, is intimately linked to the atmospheric circulation over the Arctic that drives the sea ice.

References

DeRepentigny, P., Tremblay, L. B., Newton, R., & Pfirman, S. (2016). Patterns of Sea Ice Retreat in the Transition to a Seasonally Ice-Free Arctic. *Journal of Climate*, *29*(19), 6993–7008. doi: https://doi.org/10.1175/JCLI-D-15-0733.1

Meier, W., Fetterer, F., Savoie, M., Mallory, S., Duerr, R., & Stroeve, J. (2017). NOAA/NSIDC Climate Data Record of Passive Microwave Sea Ice Concentration, Version 3 Revision 1 [monthly averages from January 1989 to December 2008]. *National Snow and Ice Data Center, Boulder, Colorado, USA*, Accessed July 2018. doi: https://doi.org/10.7265/N59P2ZTG

Newton, R., Pfirman, S., Tremblay, B., & DeRepentigny, P. (2017). Increasing transnational sea-ice exchange in a changing Arctic Ocean. *Earth's Future*, *5*(6), 633–647. doi: https://doi.org/10.1002/2016EF000500

Peng, G., Meier, W., Scott, D., & Savoie, M. (2013). A long-term and reproducible passive microwave sea ice concentration data record for climate studies and monitoring. *Earth System Science Data*, *5*(2), 311–318. doi: https://doi.org/10.5194/essd-5-311-2013

Tschudi, M., Fowler, C., Maslanik, J., Stewart, J. S., & Meier, W. (2016). Polar Pathfinder Daily 25 km EASE-Grid Sea Ice Motion Vectors, Version 3 [monthly averages from January 1989 to December 2008]. *NASA National Snow and Ice Data Center Distributed Active Archive Center, Boulder, Colorado, USA*, Accessed March 2016. doi: http://dx.doi.org/10.5067/O57VAIT2AYYY

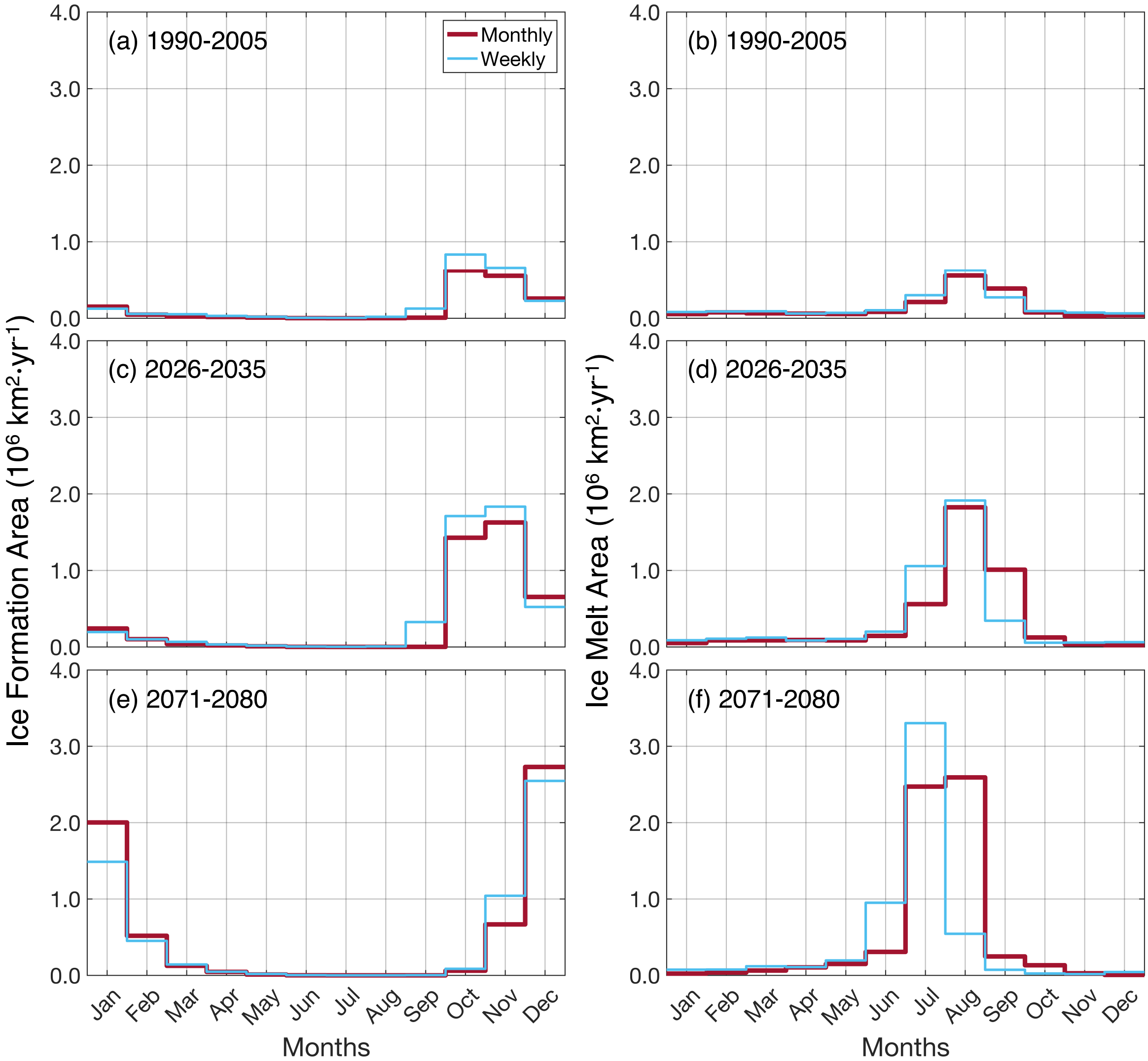

Figure S1: Annual cycle of ice formation (a, c, e) and melt (b, d, f) over the periods of 1990–2005 (a, b), 2026–2035 (c, d) and 2071–2080 (e, f) for the first 35 members of the CESM-LE using a monthly (burgundy) and weekly (light blue) time resolutions. Only ice floes that formed and melted between the specified time periods are considered. Note that some of the differences between the weekly and monthly time resolution can be attributed to the way weeks are distributed into months as every month contains either 29, 30 or 31 days and thus always includes part of a week.

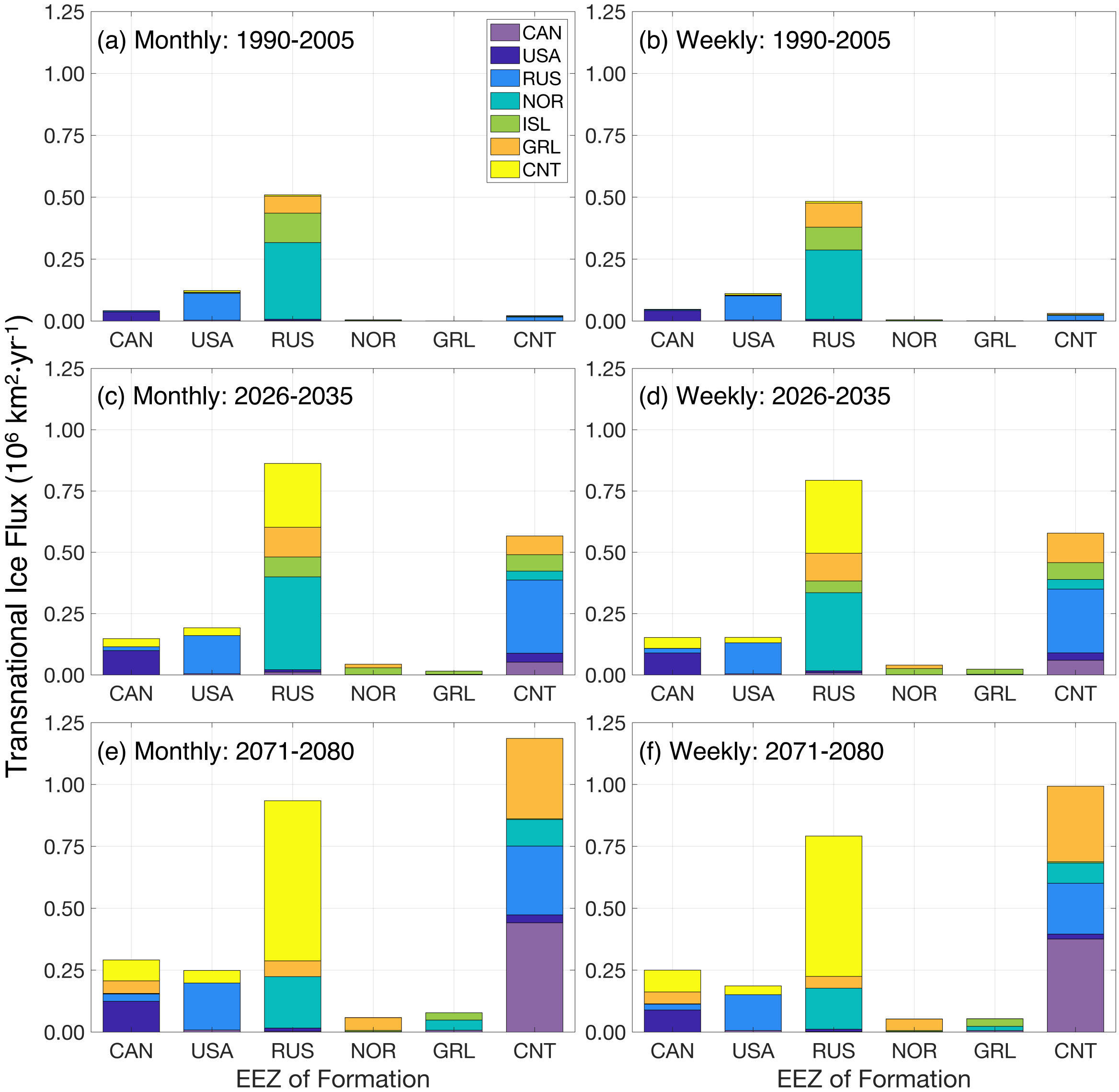

Figure S2: Annual mean average areal flux of transnational ice for the CESM-LE over the periods of 1990–2005 (a, b), 2026–2035 (c, d) and 2071–2080 (e, f) using a monthly (a, c, e) and weekly (b, d, f) time resolutions. The height of each colored portion within one bar represents the annual mean areal flux of ice between the EEZ of formation (x axis) and the EEZ of melt (color). Note that domestic ice is not included in this figure in order to focus on the features of transnational ice exchange.

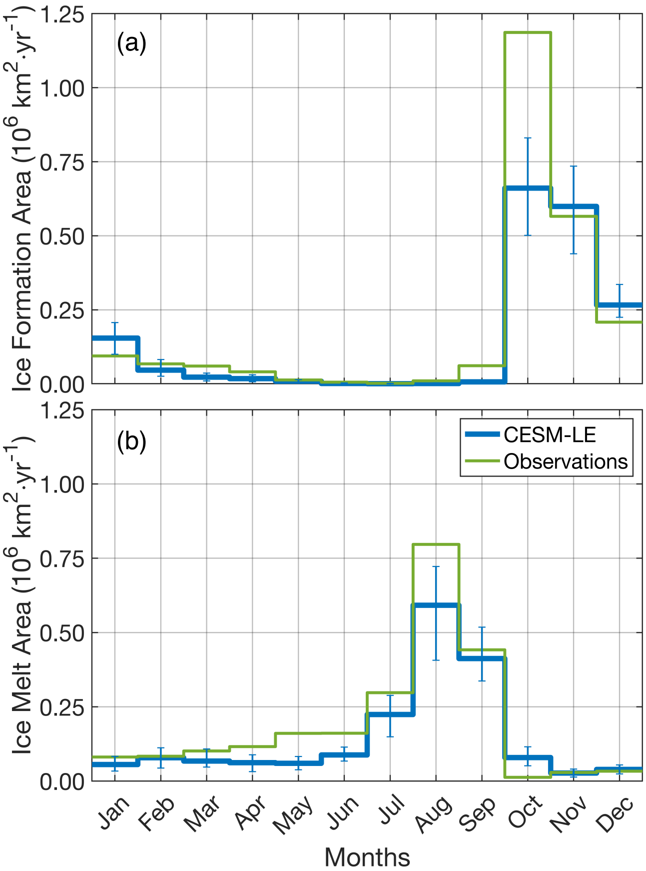

Figure S3: Annual cycle of mean areal ice formation (a) and melt (b) in the observations (green) and the CESM-LE (blue) for the period of 1989–2008. The error bars show the maximum and minimum 20-year averaged formation/melt area for each month across the 40 ensemble members of the CESM-LE, showing the range of internal variability for this ensemble. Only ice floes that formed and melted between 1989–2008 are considered. Note that the values shown here are not meant to represent the actual amount of ice that forms and melts in the Arctic every year, but rather the area of ice formation and melt we obtain from SITU (see section 2.2).

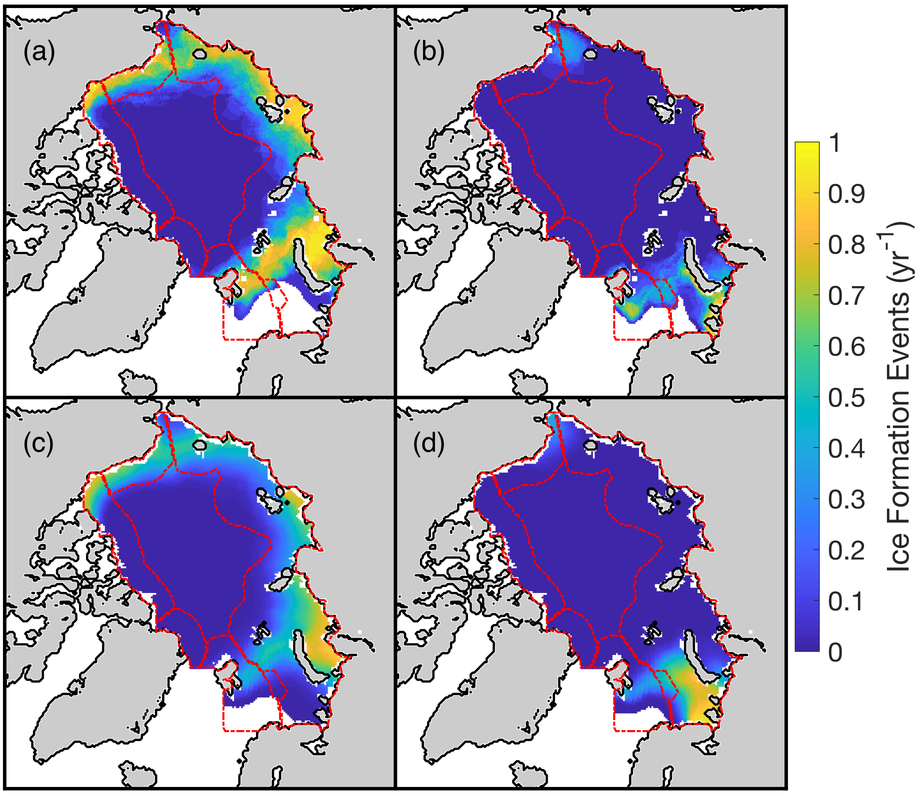

Figure S4: Average number of ice formation events per year in fall (SON) (a, c) and winter (DJF) (b, d) over the period of 1989–2008 for both observations (a, b) and the CESM-LE (c, d). The borders of the EEZs are indicated by red lines. Only ice floes that formed and melted between 1989–2008 are considered.

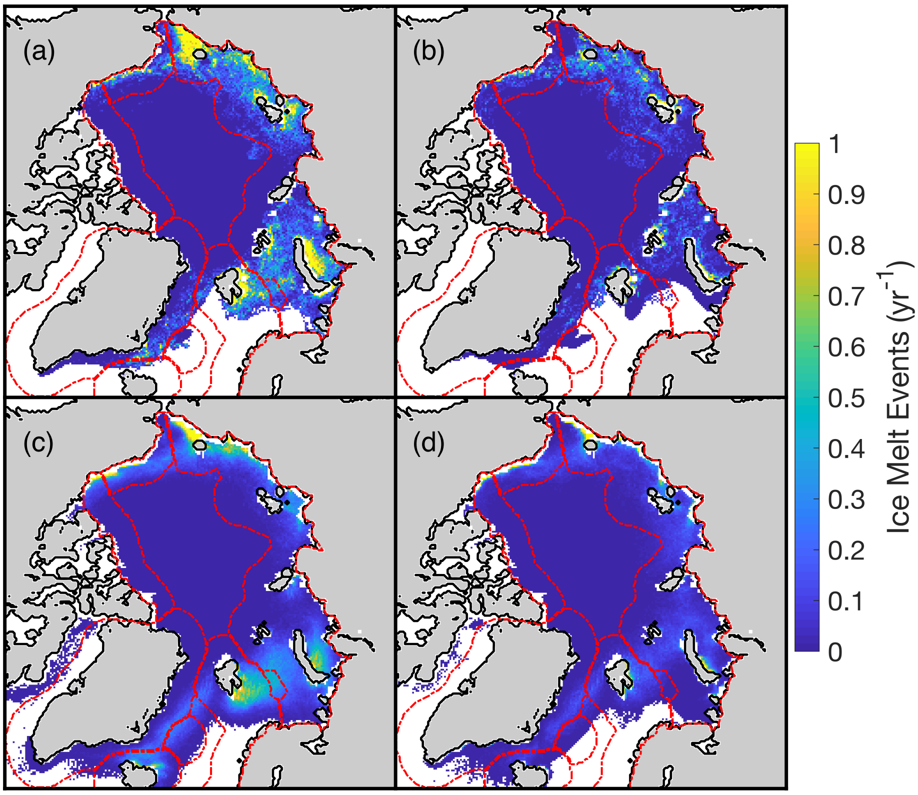

Figure S5: As in Figure S4, but for the average number of ice melt events per year in summer (JJA) (a, c) and fall (SON) (b, d).

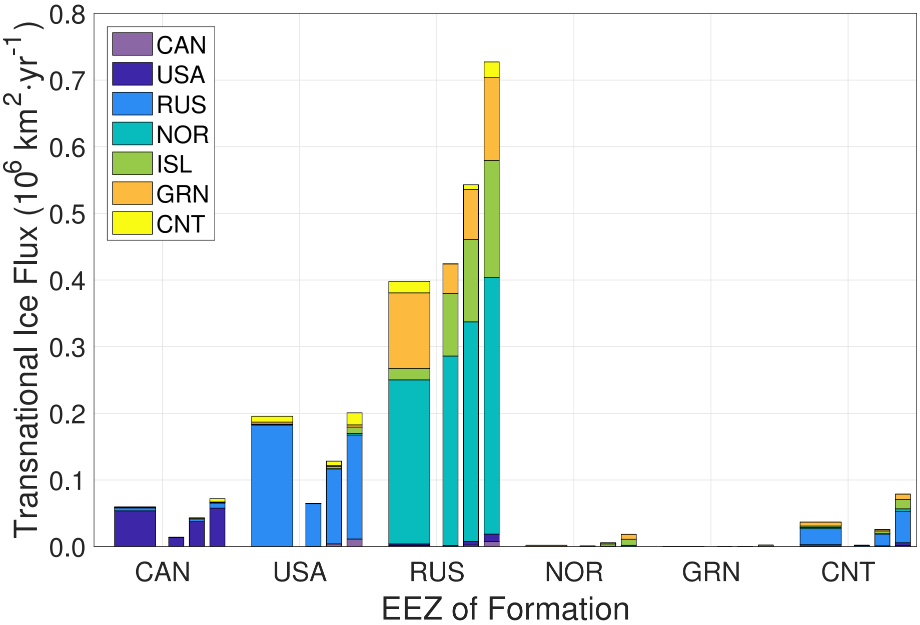

Figure S6: Annual mean areal transnational ice flux for the observations (wide bar) and annual mean minimum (left narrow bar), average (middle narrow bar) and maximum (right narrow bar) areal transnational ice flux for the 40 members of the CESM-LE for the period of 1989–2008. The height of each colored portion within one bar represents the annual mean areal flux of ice between the EEZ of formation (x axis) and the EEZ of melt (color). The CESM-LE is consistent with the observations when the observed value for each pathway lies between the range of the CESM-LE (minimum to maximum). Note that domestic ice is not included in this figure in order to focus on the features of transnational ice exchange.

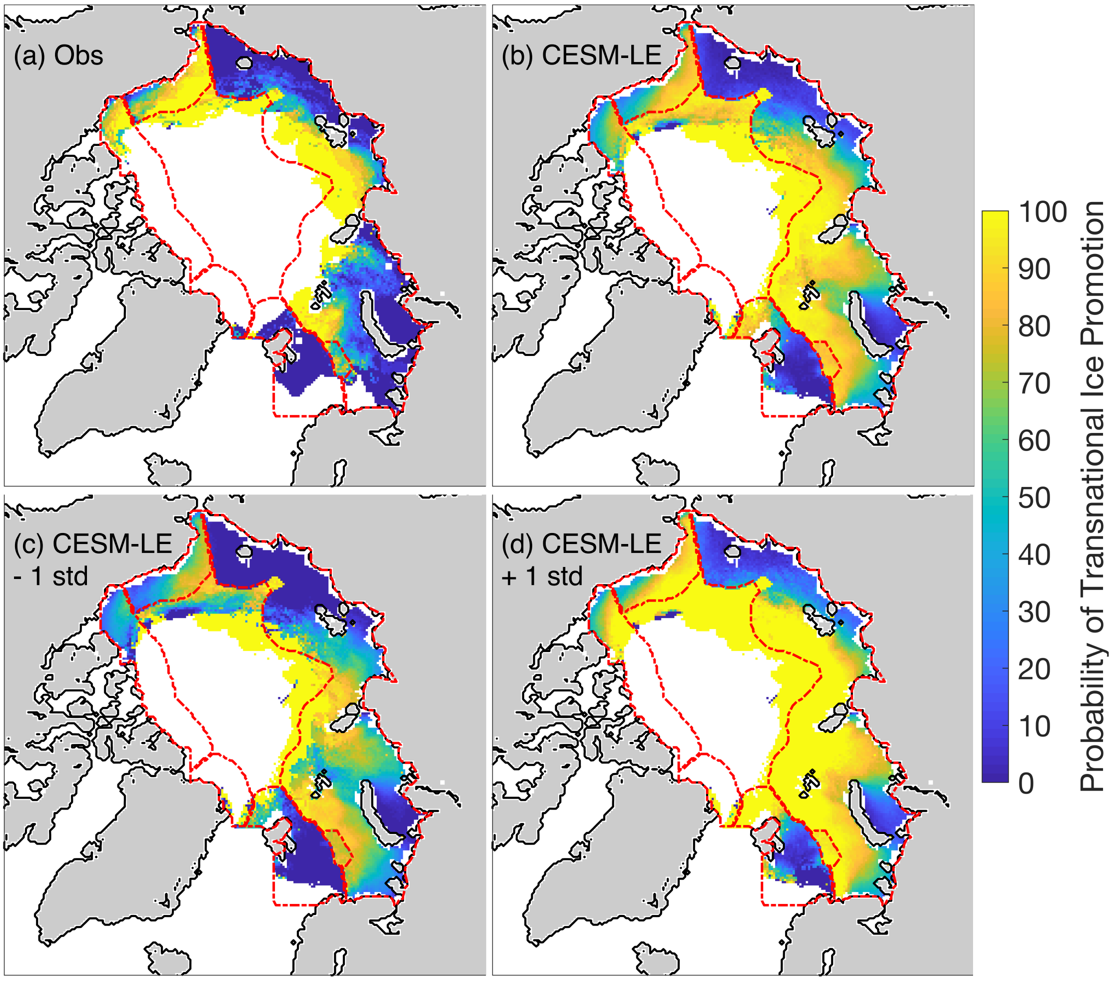

Figure S7: Probability of transnational ice promotion for observations (a), the ensemble mean of the CESM-LE (b) as well as the ensemble mean ± one standard deviation for the CESM-LE (c, d) over the period of 1989–2008. The color represents the probability that an ice parcel forming at each grid cell gets promoted from domestic ice to transnational ice. The borders of the EEZs are indicated by red lines. Note that the probability is calculated for each grid cell in which at least one ice parcel forms and thus gives no indication of how many ice parcels are considered in the calculation.

Table S1: Annual mean average areal flux of ice exchanged between all EEZs for the CESM-LE over the three time periods. The EEZ of formation is indicated in the first column and the EEZ of melt in the first row. All numbers are in km^2/year. The last column contains the total annual mean average areal flux of ice formed in each EEZ, only considering ice floes that melted before the end of the time period. The numbers in bold highlight the pathways that are statistically different between the CESM-LE and the CESM-LW over a same time period at the 95% confidence level using a t-test.

From/To	*Canada*	*USA*	*Russia*	*Norway*	*Iceland*	*Greenland*	*Central*	*Total*
1981–2000								
Canada	39,426	32,741	3,177	32	218	96	631	76,321
USA	3,616	49,083	96,402	546	4,232	1,444	4,184	159,507
Russia	1,635	4,900	563,494	305,730	112,159	60,825	2,217	1,050,960
Norway	0	0	677	108,733	2,331	1,223	0	112,964
Greenland	0	0	0	4	113	31	0	148
Central	163	802	9,026	292	1,585	581	934	13,383
2031–2050								
Canada	107,566	128,998	25,926	441	**1,563**	**4,855**	**62,049**	331,398
USA	6,297	105,809	176,848	0	**0**	0	**34,613**	323,567
Russia	**11,480**	10,188	1,597,911	**385,601**	**37,521**	**122,715**	**452,339**	2,617,755
Norway	10	0	737	135,196	33,191	**31,475**	18	200,627
Greenland	**789**	11	8	**10,823**	**41,205**	27,128	51	80,015
Central	**184,175**	52,953	352,701	**69,168**	81,513	**194,498**	833,752	1,768,760
2081–2100								
Canada	327,395	**114,877**	33,716	**3,209**	**175**	**70,427**	**102,810**	652,609
USA	6,742	66,614	184,671	0	0	0	**60,638**	318,665
Russia	**2,495**	**13,346**	1,429,691	**162,929**	**4**	**40,631**	**654,681**	2,303,777
Norway	9	0	**1,692**	91,323	**1,331**	38,416	**821**	133,592
Greenland	**7,436**	**0**	64	**41,848**	**13,268**	177,128	603	240,347
Central	**437,773**	**17,441**	**250,289**	**111,080**	**410**	**310,993**	1,360,152	2,488,138

Table S2: As in Table S1, but for the CESM-LW and for the time periods of 2031–2050 and 2081–2100 only.

From/To	*Canada*	*USA*	*Russia*	*Norway*	*Iceland*	*Greenland*	*Central*	*Total*
2031–2050								
Canada	67,835	116,784	28,938	9	**401**	**423**	**38,568**	252,958
USA	4,134	102,824	181,077	3	**28**	20	**20,594**	308,680
Russia	**17,224**	13,310	1,529,744	**416,960**	**73,301**	**137,656**	**311,557**	2,499,752
Norway	0	0	918	137,622	29,449	**24,446**	0	192,435
Greenland	**97**	0	0	**4,560**	**25,810**	9,903	0	40,370
Central	**95,631**	53,653	357,849	**40,909**	78,207	**117,193**	540,412	1,283,854
2081–2100								
Canada	84,594	**139,616**	41,702	**85**	**1,153**	**2,207**	**67,080**	336,437
USA	3,884	95,500	196,153	0	0	0	**25,227**	320,764
Russia	**16,006**	**8,551**	1,600,756	**386,994**	**38,009**	**153,526**	**428,526**	2,632,368
Norway	51	0	**739**	130,358	**38,855**	35,565	**0**	205,568
Greenland	**1,307**	**125**	6	**8,969**	**51,634**	24,952	57	87,050
Central	**192,349**	**55,827**	**411,670**	**53,332**	**84,082**	**189,324**	813,423	1,800,007